R. & M. No. 3751

R. & M. No. 3751

PROCUREMENT EXECUTIVE, MINISTRY OF DEFENCE

AERONAUTICAL RESEARCH COUNCIL
REPORTS AND MEMORANDA

Computation of the Velocity Field Induced by a Planar Source Distribution Approximating a Symmetrical Non-Lifting Wing in Subsonic Flow

By J. A. Ledger
Aerodynamics Dept., R.A.E., Farnborough

LONDON: HER MAJESTY'S STATIONERY OFFICE
1974
PRICE £1·65 NET

Computation of the Velocity Field Induced by a Planar Source Distribution Approximating a Symmetrical Non-Lifting Wing in Subsonic Flow

By J. A. Ledger

Aerodynamics Dept., R.A.E., Farnborough

Reports and Memoranda No. 3751*
September, 1972

Summary

The singular double integrals which arise in the calculation of the components of perturbation velocity due to a swept wing with given thickness distribution by linearised theory, have been evaluated by a numerical method. Two computer programs have been written, one for points on the wing planform and one for points off.

Following the techniques adopted by Sells, the integral over the wing is constructed from the sum of analytic spanwise integrals taken along lines of local sweep.

The results obtained were tested against calculations by Freestone for points on the wing planform for both sheared and tapered wings. Further comparisons for points on the wing surface were made with results by the method of A. M. O. Smith.

* Replaces R.A.E. Technical Report 72176—A.R.C. 34 383

LIST OF CONTENTS

1. Introduction

The basic equation of linearised theory for a thick, symmetrical, non-lifting wing in subsonic flow gives the perturbation potential at any point as a double integral of the surface slope over the wing planform. By differentiation, the three components of perturbation velocity may be determined, but to make this calculation, a very large number of double integral evaluations may have to be performed and the complex nature of the wing geometry will necessarily preclude any general attempt at an analytic analysis.

We recognise that the objective of this work is to improve design methods for wings and wing-fuselage combinations, which will necessitate the prediction of the flow field produced by the wing, both on and off its surface. Within this general framework, the calculation of velocities due to thickness is but one stage and so we should seek a method which is compatible with an accurate and tested method of predicting velocities due to a given doublet (loading) distribution; in this case the method of Sells.[1]

The existing methods of solving the thickness problem are tailored to predicting the velocity field in special regions of space, e.g. Freestone[2] for velocities on the wing planform ($z = 0$), A. M. O. Smith[6] for wing surface velocities; but we aim to be quite unrestrictive and have developed a method which will predict the velocity field everywhere (the only point of failure being the apex of a swept wing).

The present method has some advantages in speed and accuracy over the method of Freestone, since we have avoided some of his difficulties by choosing (as with Sells[1]), a coordinate system matched to the wing planform so that a high level of numerical refinement in evaluating integrals near the leading and trailing edges is unnecessary.

The program is written for incompressible flows and application to subsonic flows is made *via* the Prandtl–Glauert (Göthert) rule.

Having thus calculated the compressible perturbation velocities to first order, it would then be desirable to make some allowance for higher-order compressibility effects by using empirical compressibility factors as in the R.A.E. standard method (*see* for example Ref. 7); in this way, reasonable accuracy for the velocity and pressure distribution on a typical moderately swept wing can be expected up to the critical Mach number, except possibly in the immediate vicinity of the central 'cranked' station (*cf.* Ref. 8).

It should be recognised that since the method provides a nominally exact means of calculating the velocity field of *any* planar source distribution (in incompressible flow), it can conveniently be used as a basis for second-order theory, as explained in Ref. 9. It is also proposed to use the method as an essential step in developing an analogous theory for wing-fuselage interference, thus generalising the procedure described in Ref. 10.

2. Linear Theory

Our objective is to estimate the velocity potential, and hence the components of perturbation velocity, induced by the presence of a symmetrical wing of small thickness-chord ratio at zero incidence in a subsonic flow. The calculations are performed assuming the flow to be incompressible, and the extension to the subsonic flow is then achieved by using the Prandtl–Glauert (Göthert) rule.

Orthogonal Cartesian axes are taken, centred on the wing apex with Ox downstream, Oy to starboard and Oz upwards, so that the wing mean plane is $z = O$.

Now let the perturbation potential be Φ, giving rise to a perturbation velocity field $\mathbf{u} = \nabla\Phi$, superposed on the uniform free stream $(U_\infty, 0, 0)$. The governing equation is then

$$\nabla^2\Phi = 0 \tag{1}$$

subject to the boundary condition that the body is a stream surface, giving

$$\frac{dx}{U_\infty + u} = \frac{dy}{v} = \frac{dz}{w} \tag{2}$$

on the wing surface, where (u, v, w) are the three components of the vector $\mathbf{u}$.

We may regard $\mathbf{u}$ as the velocity induced by a planar distribution of sources on the plane $z = 0$, of strength $q(x, y)$ per unit area; $\mathbf{u}$ is regular except at some points on $z = 0$. Then we may write

$$w(z = z_t) = w(z = 0) + O(\tau) \tag{3}$$

where $z = z_t(x, y)$ is the equation of the wing surface, and we assume

$$\tau = \frac{(z_t)_{\max}}{c} \ll 1.$$

Now $w(x, y, 0) = \pm\frac{1}{2}q(x, y)$ on $z = \pm 0$; hence, using equations (2) and (3) together with the approximation

$$\left.\begin{aligned} u &= U_\infty + \tau u_1 + \dots \\ v &= \tau v_1 + \dots \\ w &= \tau w_1 + \dots \end{aligned}\right\} \tag{4}$$

where

$$u_1 = \frac{\partial \Phi}{\partial x}, \qquad v_1 = \frac{\partial \Phi}{\partial y}, \qquad w_1 = \frac{\partial \Phi}{\partial z} \tag{5}$$

we obtain, to first order

$$q(x, y) = 2U_\infty \frac{\partial z_t(x, y)}{\partial x}, \tag{6}$$

where $2z_t(x, y)$ is the thickness of the (symmetrical) wing section.

Now, for a source of strength $q(x', y')$ per unit area at a point (x', y'), the velocity potential at a point (x, y, z) is the solution of Laplace's equation given by

$$d\Phi(x, y) = d\Phi = -\frac{1}{4\pi} q(x', y') \frac{1}{r}\, dx'\, dy', \tag{7}$$

where $r^2 = (x - x')^2 + (y - y')^2 + z^2$.

Hence, for the whole wing

$$\Phi(x, y, z) = -\frac{1}{4\pi} \iint_{z=0} q(x', y') \frac{1}{r}\, dx'\, dy', \tag{8}$$

where $q = 2U_\infty\, dz_t/dx$.

Since, of course, $q(x, y)$ is zero off the wing planform, the integration may be restricted to this area only.

The three components of perturbation velocity are given by

$$u(x, y, z) = +\frac{1}{4\pi} \iint_{\text{wing}} q(x', y') \frac{(x - x')}{r^3}\, dx'\, dy', \tag{9}$$

$$v(x, y, z) = +\frac{1}{4\pi} \iint_{\text{wing}} q(x', y') \frac{(y - y')}{r^3}\, dx'\, dy' \tag{10}$$

and

$$w(x, y, z) = +\frac{1}{4\pi} \iint_{\text{wing}} q(x', y') \frac{z}{r^3}\, dx'\, dy'. \tag{11}$$

3. Transformation of Coordinates

When the planform and surface slope of the wing are given, we wish to evaluate equations (9), (10) and (11) for z both zero and non-zero. We will usually be dealing with wings having sections with rounded leading edges, hence the kernel of the integrals above will have an inverse square root singularity and, in addition, there will generally be a pole of order two at the field point $(x, y, 0)$.

Also, when z is small (*cf.* Sells[1]), the integral will not be well-behaved numerically near $y = y'$. We aim to obviate these difficulties by dividing the wing up into thin chordwise strips (*see* Fig. 1), across which a simple quadratic representation of the source function will be sufficiently accurate, enabling a spanwise analytic integration to be performed following the local sweep. This leaves the chordwise integration to be done numerically.

The surface slopes are specified as data along the partition lines y = constant, which are chosen subject to the following conditions.

(1) The centreline shall be the first partition line.

(2) With the integration being carried out, in general, across three lines, the control line (*see* Figs. 1 and 2) should fall strictly between the two bounding partition lines.

(3) Near the root where, on many wings, there is a rapid variation of thickness with spanwise displacement necessitated by aerodynamic and structural considerations, the partition lines should be grouped more closely in order to obtain a better definition of the spanwise variation.

(4) In the vicinity of a rounded tip, the last outboard partition strip should be made as small as possible to avoid errors associated with a spanwise variation of surface slope like $O(1 - \eta^2)^{\frac{1}{2}}$ as $\eta \to \pm 1$, which, for accurate treatment, would entail the use of elliptic integrals which we propose to avoid, in order to minimise computing times.

Firstly, we introduce a new chordwise variable, ϕ (as in Ref. 1), to replace x, so that the new coordinate system is tailored to the wing planform by making the leading and trailing edges into coordinate lines.

The transformation is

$$x' = x_l(y') + \tfrac{1}{2}c(y')(1 - \cos\phi) \tag{12}$$

and is used in the R.A.E. standard method. The leading edge corresponds to $\phi = 0$ and the trailing edge to $\phi = \pi$.

Then, from equation (8),

$$\Phi(\phi, y, z) = -\sum_{\text{all strips}} \frac{1}{4\pi} \int_0^{\pi} \tfrac{1}{2}\, d\phi \int_{\text{strip}} Q(\phi, y') \frac{1}{r}\, dy', \tag{13}$$

where $Q(\phi, y') = q(x', y')c(y') \sin\phi$.

Near the leading edge ($\phi = 0$),

$$\sin\phi \backsim (x' - x_l)^{\frac{1}{2}} \tag{14}$$

and

$$q(x', y') \backsim (x' - x_l)^{\frac{1}{2}}, \tag{15}$$

so that $Q(\phi, y')$ is bounded at the leading edge.

Furthermore, at the trailing edge ($\phi = \pi$), $Q(\phi, y')$ is finite (and zero) and well-behaved at $\phi = \pi$, for zero or finite $q(x', y')$ so that $Q(\pi, y')$ can be used in a computer program.

For the spanwise integration, we shift the origin to the control point (x, y, z) and define a new variable

$$\eta = y' - y \tag{16}$$

and adjust the limits of integration accordingly across the typical strip.

On this typical integration strip, bounded by $\eta = \eta_+$ and $\eta = \eta_-$ (*see* Fig. 2), we choose a reference line $y' = y^*$ and on each line ϕ = constant, we replace Q by its three term Taylor expansion about this line, thus

$$Q = G_0^* + (y' - y^*)G_1^* + (y' - y^*)^2 G_2^* \tag{17}$$

where G_0^*, G_1^* and G_2^* are evaluated on the reference line and thus depend only on quantities not related to the control point. To obtain a representation of Q valid in the strip $\eta_- \leqslant \eta \leqslant \eta_+$ (Fig. 2) we rearrange equation (16) thus

$$y' - y^* = \eta + y - y^*. \tag{18}$$

Inserting (18) into (17), we obtain

$$\begin{aligned} Q &= G_0^* + (\eta + y - y^*)G_1^* + (\eta + y - y^*)^2 G_2^* \\ &= [G_0^* + (y - y^*)G_1^* + (y - y^*)^2 G_2^*] + \eta[G_1^* + 2(y - y^*)G_2^*] + \eta^2 G_2^* \qquad (19) \\ &= G_0 + \eta G_1 + \eta^2 G_2 \qquad (20) \end{aligned}$$

where

$$G_0 = G_0^* + (y - y^*)G_1^* + (y - y^*)^2 G_2^*, \tag{21}$$

$$G_1 = G_1^* + 2(y - y^*)G_2^* \tag{22}$$

and

$$G_2 = G_2^*. \tag{23}$$

Now $Q = Q(\phi, y')$ from equation (13), so that G_0^*, G_1^* and G_2^* are functions of ϕ. Hence, from equations (21) to (23) G_0 and G_1 are functions of ϕ and y, and G_2 is a function of ϕ alone.

Hence for the kernel function in equation (13), we may write

$$Q(\phi, y') = G_0(\phi, y) + \eta G_1(\phi, y) + \eta^2 G_2(\phi) \tag{24}$$

valid on the strip $\eta_- \leqslant \eta \leqslant \eta_+$, even though the strip does not in general include the point $\eta = 0$ (Sells[1]).

We now introduce the local section coordinate ξ, defined by

$$x' = x_l(y') + \xi c(y') \tag{25}$$

where $\xi = \frac{1}{2}(1 - \cos\phi)$ and from this we see that the variation of $(x' - x_l)$ across a strip depends only on $x_l(y')$ and $c(y')$, and the true variation of $x_l(y')$ and $c(y')$ within a strip is approximated by a linear variation in order to make the analytic integration possible. For a more detailed discussion of this point, *see* Ref. 1. In addition, for wings with straight leading and trailing edges, x_l^* and c^* are respectively the values of the leading-edge coordinate and local chord at the control line.

If η^* is the reference point for the range $[\eta_-, \eta_+]$, we have

$$x_l(y') = x_l^* + \eta\left(\frac{\partial x_l}{\partial y'}\right)_{y' = y + \eta^*} \tag{26}$$

where

$$x_l^* = \left(x_l - \eta^* \frac{\partial x_l}{\partial y'}\right)_{y' = y + \eta^*}$$

We can write

$$x' - x = h + \eta a, \tag{27}$$

where a is independent of η for a given strip, but varies with ξ along the chord and

$$h = x_l^* + c^*\xi - x, \qquad (\textit{see} \text{ Fig. 3}) \tag{28}$$

$$c^* = \left(c - \eta^* \frac{\partial c}{\partial y'}\right)_{y' = y + \eta^*} \tag{29}$$

and

$$a = \frac{\partial x_l}{\partial y'} + \xi \frac{\partial c}{\partial y'} = \tan \Lambda_\xi, \tag{30}$$

where Λ_ξ is the angle of sweep of the line ξ = constant.
We may now write

$$\Phi(x, y, z) = -\frac{1}{4\pi} \sum_{\substack{\text{strips} \\ [\eta-, \eta+]}} \frac{1}{2} \int_0^\pi d\phi [I]_{\eta-}^{\eta+}, \tag{31}$$

where

$$I = G_0 J_0 + G_1 J_1 + G_2 J_2 \tag{32}$$

and

$$J_0 = \int \frac{1}{r} d\eta, \tag{33}$$

$$J_1 = \int \frac{\eta}{r} d\eta \tag{34}$$

and

$$J_2 = \int \frac{\eta^2}{r} d\eta. \tag{35}$$

Here,

$$\begin{aligned} r^2 &= (h + a\eta)^2 + \eta^2 + z^2 \\ &= b^2\eta^2 + 2ha\eta + h^2 + z^2 \end{aligned} \tag{36}$$

and

$$b = \sqrt{(1 + a^2)} = \sec \Lambda_\xi.$$

4. Spanwise Integration

We now evaluate the integrals (33), (34) and (35) and from these obtain equivalent expressions for the three orthogonal components of perturbation velocity which we seek.

From (33)

$$J_0 = \frac{1}{b} \ln \left(r + b\eta + \frac{ha}{b} \right), \tag{37}$$

from (34)

$$J_1 = \frac{1}{b^2} r - \frac{ha}{b^3} \ln \left(r + b\eta + \frac{ha}{b} \right) \tag{38}$$

and from (35)

$$J_2 = \frac{\eta r}{2b^2} - \frac{3ha}{2b^4} r + \frac{1}{2b^5} \{(2a^2 - 1)h^2 - b^2 z^2\} \times \ln \left(r + b\eta + \frac{ha}{b} \right). \tag{39}$$

Recalling equations (16) and (27), we obtain by differentiation

$$\frac{\partial}{\partial x} = -\frac{\partial}{\partial h}, \tag{40}$$

$$\frac{\partial}{\partial y} = a\frac{\partial}{\partial h} - \frac{\partial}{\partial \eta} \tag{41}$$

and

$$\frac{\partial}{\partial z} = \frac{\partial}{\partial z}. \tag{42}$$

We note in passing that when these new operators are applied to (37), a and b are independent of x and y and hence their derivatives with respect to h and η are zero, so that no terms depending on c and dc/dy appear in our formulae. Using (32) with (40), we find that the perturbation streamwash is given by

$$u = \frac{\partial \Phi}{\partial x}$$

$$= -\frac{1}{4\pi} \sum_{\substack{\text{strips} \\ [\eta_-, \eta_+]}} \frac{1}{2} \int_0^{\pi} d\phi \left[\frac{\partial I}{\partial x} \right]_{\eta_-}^{\eta_+} \tag{43}$$

$$= -\frac{1}{4\pi} \sum_{\substack{\text{strips} \\ [\eta_-, \eta_+]}} \frac{1}{2} \int_0^{\pi} d\phi \left[\frac{\partial}{\partial x}(G_0 J_0 + G_1 J_1 + G_2 J_2) \right]_{\eta_-}^{\eta_+} \quad \text{by (31)} \tag{44}$$

$$= -\frac{1}{4\pi} \sum_{\substack{\text{strips} \\ [\eta_-, \eta_+]}} \frac{1}{2} \int_0^{\pi} d\phi \left[\sum_{n=0}^{2} \left\{ \frac{\partial G_n}{\partial x} J_n - G_n \frac{\partial J_n}{\partial h} \right\} \right]_{\eta_-}^{\eta_+} \quad \text{by (40)} \tag{45}$$

$$= -\frac{1}{4\pi} \sum_{\substack{\text{strips} \\ [\eta_-, \eta_+]}} \frac{1}{2} \int_0^{\pi} d\phi \left[-\sum_{n=0}^{2} G_n \frac{\partial J_n}{\partial h} \right]_{\eta_-}^{\eta_+} \tag{46}$$

where, after some manipulation using equations (37), (38) and (39) we find that the term in equation (46) contained in the square brackets reduces to

$$G_0 \left\{ \frac{1}{h^2 + b^2 z^2} \frac{h\eta - az^2}{r} \right\} +$$

$$+ G_1 \left\{ \frac{a}{b^3} \ln \left(r + b\eta + \frac{ha}{b} \right) - \frac{1}{b^2 r (h^2 + b^2 z^2)} [a(2h^2 + b^2 z^2)\eta + h(h^2 + z^2)] \right\} +$$

$$+ G_2 \left\{ \frac{h}{b^5}(1 - 2a^2) \ln \left(r + b\eta + \frac{ha}{b} \right) + \frac{1}{b^2 r (h^2 + b^2 z^2)} \left[a(h^2 + b^2 z^2)\eta^2 + \frac{1}{b^2} \times \right. \right.$$

$$\left. \left. \times \{h^3(5a^2 - 1) + h(4a^2 - 1)b^2 z^2\}\eta + \frac{a}{b^2}(3h^2 + 2b^2 z^2)(h^2 + z^2) \right] \right\}$$

$$= \chi, \quad \text{say} \quad . \tag{47}$$

In a similar way, the formula for the sidewash $v(x, y, z)$ is obtained from

$$v = \frac{\partial \Phi}{\partial y}$$

$$= -\frac{1}{4\pi} \sum_{\substack{\text{strips} \\ [\eta_-, \eta_+]}} \frac{1}{2} \int_0^{\pi} d\phi \left[\frac{\partial}{\partial y}(G_0 J_0 + G_1 J_1 + G_2 J_2) \right]_{\eta_-}^{\eta_+} \quad \text{by (31)} \tag{48}$$

$$= -\frac{1}{4\pi} \sum_{\text{strips}} \frac{1}{2} \int_0^{\pi} d\phi \left[\sum_{n=0}^{2} \left\{ G_n \left(a \frac{\partial J_n}{\partial h} - \frac{\partial J_n}{\partial \eta} \right) + J_n \frac{\partial G_n}{\partial y} \right\} \right]_{\eta_-}^{\eta_+}. \tag{49}$$

Now, differentiating equations (21), (22) and (23) with respect to y,

$$\frac{\partial G_0}{\partial y} = G_1^* + 2(y - y^*)G_2^* = G_1(\phi, y), \tag{50}$$

$$\frac{\partial G_1}{\partial y} = 2G_2^* = 2G_2(\phi, y) \tag{51}$$

and

$$\frac{\partial G_2}{\partial y} = 0. \tag{52}$$

Substituting these expressions into (49), we obtain

$$v = -\frac{1}{4\pi} \sum_{\substack{\text{strips} \\ [\eta_-, \eta_+]}} \frac{1}{2} \int_0^\pi d\phi \left[\sum_{n=0}^{2} G_n \left(a \frac{\partial J_n}{\partial h} - \frac{\partial J_n}{\partial \eta} \right) + G_1 J_0 + 2G_2 J_1 \right]_{\eta_-}^{\eta_+} \tag{53}$$

where the term in (53) in square brackets is

$$\begin{aligned} & G_0 \left\{ - \frac{1}{h^2 + b^2 z^2} \frac{ah\eta + h^2 + z^2}{r} \right\} + \\ & + G_1 \left\{ \frac{1}{b_3} \ln \left(r + b\eta + \frac{ha}{b} \right) + \frac{1}{b^2(h^2 + b^2 z^2) r} [(h^2(a^2 - 1) - b^2 z^2)\eta + ha(h^2 + z^2)] \right\} + \\ & + G_2 \left\{ - \frac{3ah}{b^5} \ln \left(r + b\eta + \frac{ha}{b} \right) + \frac{1}{b^4 r} \left[b^2\eta^2 + 5ha\eta + 2(h^2 + z^2) - \frac{a^2 h^2}{h^2 + b^2 z^2} (ah\eta + h^2 + z^2) \right] \right\} \\ & = \Delta, \quad \text{say.} \end{aligned} \tag{54}$$

The upwash, $w(x, y, z)$ due to the displacement effect is given by

$$\begin{aligned} w &= \frac{\partial \Phi}{\partial z} \\ &= -\frac{1}{4\pi} \sum_{\substack{\text{strips} \\ [\eta_-, \eta_+]}} \frac{1}{2} \int_0^\pi d\phi \left[\frac{\partial I}{\partial z} \right]_{\eta_-}^{\eta_+}, \end{aligned}$$

where

$$\begin{aligned} \frac{\partial I}{\partial z} = & \frac{z}{r(h^2 + b^2 z^2)} \{ - G_0(ha + b^2\eta) + G_1(ha\eta + h^2 + z^2) \} - \\ & - G_2 \left[\frac{z}{b^3} \ln \left(r + b\eta + \frac{ha}{b} \right) + \frac{z}{b^2 r(h^2 + b^2 z^2)} \{ (h^2(a^2 - 1) - b^2 z^2)\eta + ha(h^2 + z^2) \} \right]. \end{aligned} \tag{55}$$

The formulae (43) to (55) are now used on each strip in turn and by summation the integral for the whole wing is built up. These formulae are evaluated at every chordwise station on each strip, and moreover, at each interpolated chordwise station near the control strip, in order to improve the accuracy there.

5. The Classical Case $z = 0$, $y \neq 0$

Since we are only concerned with symmetrical wings in this report, the upwash due to thickness, on the wing planform ($z = 0+$) is $\frac{1}{2}q(x, y)$, and so we are only required to compute $u(x, y, 0)$ and $v(x, y, 0)$.

For the reasons put forward by Sells[1] we proceed as follows in the evaluation of (47) and (54) for $z = 0$. The finite part of the singular spanwise integral is obtained by retaining $z \neq 0$, carrying out the crucial spanwise integration across the control strip, and then letting $z \to 0$.

If we put $z = 0$ in (47), we obtain, for the integrand in the expression for the streamwise perturbation velocity,

$$(\chi)_{z=0} = \left[-\frac{\partial I}{\partial h}\right]_{z=0} = G_0\frac{\eta}{hr_0} + \frac{1}{b^3}\left\{G_1 a + G_2\frac{h}{b^2}(1 - 2a^2)\right\}\ln\left(r_0 + b\eta + \frac{ha}{b}\right) -$$

$$- G_1\frac{1}{b^2 r_0}(2a\eta + h) + G_2\frac{1}{b^2 r_0}\left\{a\eta^2 + \frac{h}{b^2}(5a^2 - 1)\eta + \frac{3ah^2}{b^2}\right\} \tag{56}$$

where

$$r_0^2 = (h + a\eta)^2 + \eta^2. \tag{57}$$

The expression (56) contains two singularities which must be removed before any numerical chordwise integration can be attempted. The first singularity is associated with the term $G_0\eta/hr_0$ and appears on the control strip where $h = 0$ (i.e. at the control point itself).

If we write

$$\chi_{10} = G_0(\phi)\left[\frac{\eta}{hr_0}\right]_{\eta_-}^{\eta_+} \tag{58}$$

and use the fact that $\eta^* = 0$ in equation (26), we find that ξ is given by

$$x_l(y) + c(y)\xi = x \tag{59}$$

when $h = 0$, and since by equation (28), h varies linearly with ξ, the integral

$$\int_0^\pi \chi_{10}\, d\phi \tag{60}$$

has a simple Cauchy principal value.

At this juncture, it is appropriate to mention that the wellknown result for infinite swept wings may be obtained as a direct consequence of the integral (60). We wish to show that the increment in velocity perpendicular to the sweep on a sheared wing is the same as that on the corresponding two-dimensional wing.

Using equation (20) with $G_1 = G_2 = 0$,

$$Q(\phi, y') = Q(\phi) = G_0(\phi) \tag{61}$$

and inserting the limits $\eta_+ = +\infty, \eta_- = -\infty$ in equation (58);

$$\lim_{\eta\to\infty}\left[\frac{\eta}{hr_0}\right]_{\eta_-}^{\eta_+} = \frac{2}{bh}. \tag{62}$$

So, combining equation (46) and integral (60) and reverting to (x, y) coordinates, we find that the increment in velocity perpendicular to the sweep is

$$\frac{U_s}{U_\infty} = \frac{1}{\pi}\int_{x_L}^{x_T}\frac{dz}{dx'}\frac{dx'}{x - x'} \tag{63}$$

which is the familiar two-dimensional result.

We now continue with the business of integrating equation (58) across the chord for any general strip on which $G_0 = G_0(\phi)$. If we look first at

$$G_0(\phi)\left[\frac{\eta}{r_0}\right]_{\eta_-}^{\eta_+} = \vartheta \qquad \text{say,} \tag{64}$$

it is apparent that this function has a value at the control point which is given by

$$\lim_{h\to 0} \vartheta = \vartheta_c = G_0(\phi_c) b_c^{-1} (\operatorname{sgn} \eta_+ - \operatorname{sgn} \eta_-), \tag{65}$$

where $b_c = \sec \Lambda_\xi$.

For the control strip $\eta_+ > 0$ and $\eta_- < 0$, so that

$$\vartheta_c = \frac{2G_{0c}}{b_c}, \tag{66}$$

but on any other integration strip $\vartheta_c = 0$. With this in mind, we proceed with the chordwise integration using the function

$$\chi_{10} - \frac{1}{h}\vartheta_c = (\vartheta - \vartheta_c)\frac{1}{h} \tag{67}$$

which is seen to be regular at the control point and has a value there which may be found by the application of de l'Hospital's rule.

$$\lim_{h\to 0} \left[\frac{G_0\eta}{hr_0}\right]_{\eta_-}^{\eta_+} = \lim_{h\to 0} \left[\frac{\dfrac{\partial}{\partial h}\left(\dfrac{G_0\eta}{r_0}\right)}{\dfrac{\partial}{\partial h}(h)}\right]_{\eta_-}^{\eta_+} = \lim_{h\to 0} \frac{\partial \vartheta}{\partial h}. \tag{68}$$

Using the result

$$r_0 \frac{dr_0}{dh} = \eta a\left(1 + \eta \frac{c'}{c^*}\right) \quad \text{at} \quad h = 0 \text{ (Sells}^1\text{)} \tag{69}$$

we find that the limit works out as

$$\frac{\partial \vartheta}{\partial h} = \left[\frac{dG_0(\phi)}{d\phi}\frac{1}{b}\frac{1}{\frac{1}{2}c^* \sin\phi} - G_0(\phi)\frac{a}{b^3}\frac{dc/d\eta}{c^*}\right]_{\phi=\phi_c} (\operatorname{sgn}\eta_+ - \operatorname{sgn}\eta_-) - \left\{G_0(\phi)\left[\frac{a}{b^3}\frac{1}{|\eta|}\right]_{\eta_-}^{\eta_+}\right\}_{\phi=\phi_c}. \tag{70}$$

The first term in this expression vanishes on all strips except the one containing the control point, since it involves the factor $(\operatorname{sgn}\eta_+ - \operatorname{sgn}\eta_-)$, but the second term appears on all the integration strips. In general, we will employ equation (70) in preference to equation (67) whenever h becomes smaller than some prespecified value.

In addition, we must remember to subtract the extra contribution to the integral which this formula implies, *viz.*

$$\int_0^\pi \frac{2G_{0\pi}}{b_c}\frac{d\phi}{h}. \tag{71}$$

On the control strip, since $h = \frac{1}{2}c(\cos\phi_c - \cos\phi)$, the integral vanishes, and as it is not evaluated on any other integration strip, it makes no contribution at all to the integration process.

We now come to deal with the weaker logarithmic singularity which is of the same form as that encountered in the downwash due to a doublet distribution (*cf.* Ref. 1) and we can apply Sells' arguments directly.

The singularity is actually associated with the term

$$\frac{1}{b^3}\left(aG_1 + \frac{h}{b^2}(1 - 2a^2)G_2\right) \ln\left(r_0 + b\eta + \frac{ha}{b}\right). \tag{72}$$

On the port side of the control line, $\eta < 0$ and since $r_0 \to b|\eta|$ as $h \to 0$, $r_0 + b_{\eta_-} + ha/b \to 0$ as $h \to 0$ (on $\eta = \eta_-$) so the term (72) becomes logarithmically singular there. To deal with this, following Ref. 1, we use the

fact that

$$\left(r_0 + b\eta + \frac{ha}{b}\right)\left(r_0 - b\eta - \frac{ha}{b}\right) = \frac{h^2}{b^2} \tag{73}$$

so that the expression

$$\frac{1}{b^3}\left(aG_1 + (1 - 2a^2)\frac{h}{b^2}G_2\right)(\operatorname{sgn}\eta)\ln\left[r_0 + (\operatorname{sgn}\eta)\left(b\eta + \frac{ha}{b}\right)\right] \tag{74}$$

is identical with (72) for $\eta > 0$ (on the starboard side of the control line) but differs from (72) by a function independent of η, which may be ignored when we evaluate the definite integral, when $\eta < 0$. Thus the expression (72) may be used in the integrand for all strips on the wing. On the control strip ($\eta_- < 0, \eta_+ > 0$) a further modification is necessary. Introducing the constant from the right side of (73), we obtain in place of (74) in the integrand,

$$\chi_{11} = \frac{1}{b^3}\left(aG_1 + \frac{h}{b^2}(1 - 2a^2)G_2\right)\left\{\left[(\operatorname{sgn}\eta)\ln\left\{r_0 + (\operatorname{sgn}\eta)\left(b\eta + \frac{ha}{b}\right)\right\}\right]_{\eta_-}^{\eta_+} - 2\ln\left(\frac{|h|}{b}\right)\right\}, \tag{75}$$

where the last term in equation (75) is utilised only on the control strip, and in this case we must balance by adding

$$-\int_0^\pi \left(\frac{2a}{b^3}G_1\right)_{\phi=\phi_c} \ln|h|\, d\phi = -\left(\frac{2a}{b^3}G_1\right)_{\phi=\phi_c} \pi \ln\left(\tfrac{1}{4}c(y)\right) \tag{76}$$

to the integral (Ref. 1).

Collecting these expressions together, we obtain for equation (46)

$$u(x, y, 0) = -\frac{1}{4\pi}\left\{\sum_{\text{strips}}\int_0^\pi d\phi([u_0]_{\eta_-}^{\eta_+} + \delta[u_1]) + \lambda_1\right\} \tag{77}$$

where

$$\begin{aligned} u_0 = {} & \left[\frac{G_0\eta}{r_0} - \left(\frac{G_0}{b}\right)_{\phi=\phi_c}(\operatorname{sgn}\eta)\right]\frac{1}{h} + \\ & + \left\{\frac{G_1 a}{b^3} + \frac{G_2 h}{b^5}(1 - 2a^2)\right\}(\operatorname{sgn}\eta)\ln\left\{r_0 + (\operatorname{sgn}\eta)\left(b\eta + \frac{ha}{b}\right)\right\} - \\ & - \frac{G_1}{b^2 r_0}(2a\eta + h) + \frac{G_2}{b^2 r_0}\left\{a\eta^2 + \frac{h}{b^2}(5a^2 - 1)\eta + \frac{3ah^2}{b^2}\right\} \end{aligned} \tag{78}$$

and

$$u_1 = 2\left\{\frac{a}{b^3}G_1 + \frac{h}{b^5}(1 - 2a^2)G_2\right\}\{\ln b - \ln|h|\} + \left(\frac{2a}{b^3}G_1\right)_{\phi=\phi_c}\ln|h|, \tag{79}$$

$$\lambda_1 = -\left(\frac{2a}{b^3}G_1\right)_{\phi=\phi_c}\pi\ln\left(\tfrac{1}{4}c(y)\right), \tag{80}$$

$\delta = 1$ for the control strip, and $\delta = 0$ elsewhere.

When $h \doteqdot 0$ by equation (70), the first term in equation (78) is replaced by

$$\left[(\operatorname{sgn}\eta)\left(\frac{1}{b}\frac{dG_0/d\phi}{\frac{1}{2}c^*\sin\phi} - G_0(\phi)\frac{a}{b^3}\frac{dc/dy}{c^*}\right) - G_0(\phi)\frac{a}{b^3}\frac{1}{|\eta|}\right]_{\phi=\phi_c}. \tag{81}$$

This completes the discussion of the formulation of the analytic spanwise integral for the streamwash perturbation. We now turn our attention to the sidewash component of perturbation velocity, $v(x, y, 0)$.

Proceeding in the same way as before, we first formally take the limit $z \to 0$ in equation (54), whence we obtain

$$(\Delta)_{z=0} = G_0\left\{-\frac{1}{h}\frac{a\eta + h}{r_0}\right\} + \frac{1}{b^3}\left\{G_1 - \frac{3ha}{b^2}G_2\right\}\ln\left(r_0 + b\eta + \frac{ha}{b}\right) + \\ + G_1\left\{\frac{(a^2-1)\eta + ha}{b^2 r_0}\right\} + \frac{G_2}{b^4 r_0}\{b^2\eta^2 + ah(5-a^2)\eta + h^2(2-a^2)\}. \tag{82}$$

As before, the expression (82) possesses a chordwise singularity on the control line associated with the first term and the integral across the chord has a simple Cauchy principal value. The second term contains a weaker logarithmic singularity which is of the same form as that encountered in the streamwash perturbation formula.

Using similar arguments to those set down above, we replace the first term of the expression (82) by

$$-\frac{1}{h}\left\{G_0\frac{a\eta + h}{r_0} - \left(\frac{G_0 a}{b}\right)_{\phi=\phi_c}(\operatorname{sgn}\eta)\right\} \tag{83}$$

which is well-behaved at the control point and may be used for chordwise integration on the control strip.

The second term of the expression (82) which holds the logarithmic singularity is replaced by

$$\frac{1}{b^3}\left(G_1 - \frac{3ha}{b^2}G_2\right)(\operatorname{sgn}\eta)\ln\left\{r_0 + (\operatorname{sgn}\eta)\left(b\eta + \frac{ha}{b}\right)\right\}. \tag{84}$$

When $h \backsim 0$, the term (83) is replaced by

$$-\left(\left[(\operatorname{sgn}\eta)\left\{\frac{a}{b}\frac{dG_0/d\phi}{\frac{1}{2}c^*\sin\phi} + \frac{G_0}{b^3}\frac{dc/d\eta}{c^*}\right\} + \frac{G_0}{b^3}\left\{\frac{1}{|\eta|}\right\}\right]_{\eta-}^{\eta+}\right)_{\phi=\phi_c}. \tag{85}$$

Corporately, these results yield a formula to replace equation (54) on $z = 0$

$$v(x, y, 0) = -\frac{1}{4\pi}\left\{\sum_{\text{strips}}\int_0^{\pi} d\phi([v_0]_{\eta-}^{\eta+} + \delta[v_1]) + \lambda_2\right\}, \tag{86}$$

where

$$v_0 = -\left[G_0\left(\frac{a\eta + h}{r_0}\right) - \left(\frac{G_0 a}{b}\right)_{\phi=\phi_c}(\operatorname{sgn}\eta)\right]\frac{1}{h} + \\ + \frac{1}{b^3}\left(G_1 - \frac{3ha}{b^2}G_2\right)(\operatorname{sgn}\eta)\ln\left\{r_0 + (\operatorname{sgn}\eta)\left(b\eta + \frac{ha}{b}\right)\right\} + \\ + G_1\left\{\frac{(a^2-1)\eta + ha}{b^2 r_0}\right\} + \frac{G_2}{b^4 r_0}\{b^2\eta^2 + (5-a^2)ha\eta + h^2(2-a^2)\} \tag{87}$$

and

$$v_1 = \frac{2}{b^3}\left(G_1 - \frac{3ha}{b^2}G_2\right)(\ln b - \ln|h|) + \left(\frac{2G_1}{b^3}\right)_{\phi=\phi_c}\ln|h| \tag{88}$$

$\delta = 1$ for the control strip and $\delta = 0$ elsewhere.

$$\lambda_2 = -\left(\frac{2G_1}{b^3}\right)_{\phi=\phi_c}\pi\ln\{\tfrac{1}{4}c(y)\}. \tag{89}$$

6. Evaluation of the Streamwash* Perturbation Velocity on the Centreline

We now come to the problem of evaluating $u(x, 0, 0)$ for an aerofoil represented by a distribution of kinked source filaments in the plane $z = 0$. By symmetry, $v(x, 0, 0) = 0$ for all x and $w(x, 0, 0+) = \frac{1}{2}q(x, 0)$ according to linearised theory. Referring to Section 4, we need to evaluate equation (47) for $\eta = z = 0$, and formally taking the limit $z = 0$.

$$u(x, y, 0) = \lim_{z\to 0}\left\{-\frac{1}{4\pi}\sum_{\text{strips}}\frac{1}{2}\int_0^\pi d\phi\left[-\frac{\partial I}{\partial h}\right]_{\eta-}^{\eta+}\right\}$$

$$= -\frac{1}{4\pi}\sum_{\substack{\text{strips}\\(\eta-,\eta+)}}\frac{1}{2}\int_0^\pi d\phi\left[-\frac{\partial I_0}{\partial h}\right]_{\eta-}^{\eta+} \tag{90}$$

where $I_0 = G_0J_{00} + G_1J_{10} + G_2J_{20}$ (*see* equation (24)).

Using equation (44) with $z = 0$,

$$-\frac{\partial J_{00}}{\partial h} = -\frac{\partial J_0}{\partial h}(\phi, \eta, 0) = \frac{\eta}{hr_0}, \tag{91}$$

$$-\frac{\partial J_{10}}{\partial h} = -\frac{\partial J_1}{\partial h}(\phi, \eta, 0) = \frac{a}{b^3}\ln\left(r_0 + b\eta + \frac{ha}{b}\right) - \frac{1}{b^2r_0}(2a\eta + h) \tag{92}$$

and

$$-\frac{\partial J_{20}}{\partial h} = -\frac{\partial J_2}{\partial h}(\phi, \eta, 0) = \frac{h}{b^5}(1 - 2a^2)\ln\left(r_0 + b\eta + \frac{ha}{b}\right) +$$

$$+\frac{1}{b^2r_0}\left\{a\eta^2 + \frac{h}{b^2}(5a^2 - 1)\eta + \frac{3ah^2}{b^2}\right\}. \tag{93}$$

We may make use of these expressions for integration strips other than the first one outboard when $z = 0$, which needs be taken with $\eta_- = 0, \eta_+ > 0$, in which case equations (91) and (92) break down. When the control point is on the centreline $y = 0$, equation (43) can be written as a sum over only half the wing, and by symmetry:

$$u(x, 0, 0) = -\frac{1}{4\pi}\lim_{z\to 0}\left\{\int_0^\pi d\phi\left[-\frac{\partial I}{\partial h}\right]_0^{\eta+} + \sum_{\substack{\text{starboard}\\\text{strips,}\\\eta_- > 0}}\int_0^\pi d\phi\left[-\frac{\partial I}{\partial h}\right]_{\eta-}^{\eta+}\right\}. \tag{94}$$

Since our aim is to perform the integration for kinked source lines at the centre section, an analysis parallel to Sells[1] will not be possible and we will need to evaluate $G_0(\phi)$, $G_1(\phi)$, $G_2(\phi)$ locally on the centreline.

For $\eta = 0$, we retain $z \neq 0$ at first, and using Sells' notation, we write

$$r_1 = [r]_{\eta=0} = \sqrt{(h^2 + z^2)}. \tag{95}$$

Using equation (44) and taking the limits $\eta \to 0$ and $z \to 0$ in turn, we can calculate the contribution from the lower limit of the definite integral in the first term of equation (94).

Taking the first two terms of equation (44), we have

$$\lim_{z\to 0}\left\{G_0\left(-\frac{az^2}{(h^2 + b^2z^2)r_1}\right) + G_1\left(\frac{a}{b^3}\ln\left(r_1 + \frac{ha}{b}\right) - \frac{h(h^2 + z^2)}{b^2r_1(h^2 + b^2z^2)}\right)\right\}. \tag{96}$$

When this is inserted into equation (94), the first term to be evaluated becomes

$$\lim_{z\to 0}\int_0^\pi G_0(\phi)\left(-\frac{az^2}{(h^2 + b^2z^2)r_1}\right)d\phi. \tag{97}$$

*Streamwash is the streamwise component of perturbation velocity.

This integral is well-behaved in the limit as $z \to 0$ (Sells[1]) and takes the value

$$-\frac{4G_0(\phi_c)}{c(0)\sin\phi_c}\frac{1}{b_c}\ln(b_c + a_c). \tag{98}$$

This in fact leads to the familiar term $-4(\partial z/\partial x)\cos\Lambda_\xi(1/\pi)\ln(1 + \sin\Lambda_\xi/1 - \sin\Lambda_\xi)$ which appears in the formulae for the behaviour of u in the neighbourhood of a crank station on a swept wing.[5]

The first term in equation (94) evaluated at the upper limit is dealt with by using equation (91), although it still contains a $1/h$ singularity, so instead we use the function $(G_0\eta/r_0 - G_{0c}/b_c)1/h$ and add $\int_0^\pi G_{0c}/b_c\, d\phi/h$ to the integral in a manner similar to Section 5.

This latter term, however, is zero and so entails no extra contribution to the integral as a whole.

For the second and third term of the integrand evaluated at the upper limit in equation (94), equations (92) and (93) contain a logarithmic singularity associated with the term:

$$\left\{\frac{G_1 a}{b^3} + \frac{G_2 h}{b^5}(1 - 2a^2)\right\}\left\{\ln\left(r_0 + b\eta + \frac{ha}{b}\right) - \ln\left(|h| + \frac{ha}{b}\right)\right\}. \tag{99}$$

As $h \to 0$, (99) yields

$$-\left(\frac{G_1 a}{b^3}\right)_{\phi=\phi_c}\ln|h|, \tag{100}$$

so we must add $(G_1 a/b^3)_{\phi=\phi_c}\ln|h|$ to the integrand to render it finite everywhere, and compensate for this by subtracting

$$\int_0^\pi \left(\frac{G_1 a}{b^3}\right)_{\phi=\phi_c}\ln|h|\, d\phi \tag{101}$$

from the integral. We remember that the expression (101) has the value

$$\left(\frac{G_1 a}{b^3}\right)_{\phi=\phi_c}\pi\ln(\tfrac{1}{4}c) \text{ (see Sells' (44) to (46)).}$$

Adding up all these contributions to the integral (94), we obtain

$$\begin{aligned}\int_0^\pi d\phi\left[-\frac{\partial I_0}{\partial h}\right]_0^\eta = {} & \frac{4G_0(\phi_c)}{c(0)\sin\phi_c}\frac{1}{b_c}\ln(b_c + a_c) - \left(\frac{G_1 a}{b^3}\right)_{\phi=\phi_c}\pi\ln(\tfrac{1}{4}c) + \\ & + \int_0^\pi d\phi\left\{\left(\frac{G_0\eta}{r_0} - \frac{G_{0c}}{b_c}\right)\frac{1}{h} + \left(\frac{G_1 a}{b^3}\right)_{\phi=\phi_c}\ln|h| + \left[\frac{G_1 a}{b^3} + \frac{G_2 h}{b^5}(1 - 2a^2)\right]\times\right. \\ & \times\left[\ln\left(r_0 + b\eta + \frac{ha}{b}\right) - \ln\left(|h| + \frac{ha}{b}\right)\right] - \left[\frac{G_1}{b^2 r_0}(2a\eta + h)\right]_0^\eta + \\ & \left. + G_2\left[\frac{1}{b^2 r_0}\left\{a\eta^2 + \frac{h\eta}{b^2}(5a^2 - 1) + \frac{3ah^2}{b^2}\right\}\right]_0^\eta\right\}.\end{aligned} \tag{102}$$

The integral (102) still contains two singularities, one due to the $1/h$ term and the other due to $\ln(|h| + ha/b)$, so we will be in trouble near the control point itself where $h = 0$. We deal with the $1/h$ singularity in the usual way, by the application of de l'Hospital's rule

$$\lim_{h\to 0}\left[\frac{G_0\eta}{hr_0}\right]_0^\eta = \lim_{h\to 0}\left[\frac{\partial}{\partial h}\left(\frac{G_0\eta}{r_0}\right)\right]_0^\eta \tag{103}$$

$$= \frac{1}{b}\frac{dG_0}{d\phi}\frac{1}{\frac{1}{2}c(0)\sin\phi_c} - \frac{G_0}{b^2\eta}\frac{a[(c'/c(0))\eta + 1]}{b} \tag{104}$$

where $\eta > 0$.

The term $\ln(|h| + ha/b) - \ln|h|$ contains a jump discontinuity at $h = 0$, but the integral will be correctly handled by the trapezoidal rule, if the arithmetic mean of the two values on each 'side' of the jump is taken. Thus we replace

$$\left(\frac{G_1 a}{b^3}\right)_{\phi=\phi_c} \ln\left(\frac{|h|}{|h| + ha/b}\right) \quad \text{in the integrand by}$$

$$\left(\frac{G_1 a}{b^3}\right)_{\phi=\phi_c} \tfrac{1}{2}\left(\ln\left(\frac{h}{h - ah/b}\right) + \ln\left(\frac{h}{h + ah/b}\right)\right)$$

$$= \left(\frac{G_1 a}{b^3}\right)_{\phi=\phi_c} \ln b \quad \text{at } h = 0. \tag{105}$$

At the control point, the remaining parts of the integrand contribute,

$$G_1\left(\frac{2a}{b^3}\right) + \frac{G_2 a\eta}{b^3}. \tag{106}$$

Hence, when $h = 0$, the integrand in equation (102) should be replaced by the function

$$\left[\frac{1}{b}\frac{dG_0}{d\phi}\frac{1}{\frac{1}{2}c(0)\sin\phi_c} - \frac{G_0 a}{\eta b^3}\left(1 + \eta\frac{c'}{c(0)}\right) + \frac{G_1 a}{b^3}\ln(2b^2\eta) - \frac{2G_1 a}{b^3} + \frac{G_2 a\eta}{b^3}\right]_{\phi=\phi_c}. \tag{107}$$

7. Surface Slope Representation

7.1. Spanwise Integration

The representation of the source distribution function of equation (17) is substantially the same as the loading representation of Ref. 1, and indeed the parabola fitting is carried out in an identical manner for the general integration strip contained by three partition lines (A', B', C' in Fig. 1). The arguments of Ref. 1 Section 6.1 have, with suitable modifications to nomenclature, validity in the current problem. However, certain features are sufficiently important to bear repetition. Firstly, in order that the spanwise integrations may be performed for all the strips, the three spanwise coefficients are replaced by their expansions about $\eta = 0$, *viz.*

$$G_0 = Q(B') - E\eta^* + E'\eta^{*2},$$

$$G_1 = E - 2E'\eta^*$$

$$G_2 = E'.$$

The integration scheme now starts from the centreline $y = 0$ and proceeds outboard on the starboard side (Fig. 4), but at each stage, the contribution from the mirror image strip on the port wing is computed. When the control point lies on the centreline, we employ the fact that the wing is symmetrical and double the contribution from the starboard wing.

The program can deal effectively with planforms having kink stations in their leading and trailing edges, but in this case the spanwise partitioning must be chosen carefully such that there is at least one partition line between any two crank stations or between the centreline and a crank station.

Difficulties arise in the neighbourhood of the wing tips. There are two reasonable suppositions which we may make:

(a) that there is sharp cut-off of the source lines at $\eta = \pm 1$; or
(b) that $Q(\phi, \eta) = O[(1 - \eta^2)^{\frac{1}{2}}]$ near $\eta = \pm 1$.

The first presents no additional problems in the integration routine but may lead to a distorted representation of the streamlines in the flow just outboard of the tip. On the other hand (b) reveals a finite value for $\partial Q/\partial\eta$ at the tips—and we must fall back on the arguments of Ref. 1, Section 6.1 and seek a 'least squares' best fit over the last outboard interval. This entails a modification to the spanwise integration routine. In either case we would aim to minimise the errors incurred in this inadequate representation of the tip shape by choosing a

spanwise partitioning with as small a last outboard interval as possible. This approach will be satisfactory provided we do not require the velocity field in the immediate vicinity of the tip.

7.2. Chordwise Integration

In the neighbourhood of the control point, the singular nature of the double integral manifests itself in rapid variations which require accurate definition before any chordwise integration using the trapezoidal rule can be attempted. The chordwise refinement technique is described in Ref. 1. In general, a chord line will be split up into three distinct subranges one of which includes the control point, and in general different levels of refinement will be found necessary in each. If P' is the best number of subdivision points in a given refinement subrange, when the control point falls within P' points of the leading or trailing edge, one subrange will not appear and the integration will be over only two subranges per strip.

We now consider the various possible methods of interpolating in the x direction for values of $Q(\phi, \eta)$ in between datum values. Linear and quadratic schemes were found to be adequate for the program evaluating the velocity at field points well off the planform. However, for calculations at field points where z/c is small and on the wing planform itself, particularly on the centreline, variations of up to 5 per cent were obtained over the rear part of the chord using simple quadratic interpolation, i.e. interpolating between points p and $p + 1$ using information at points $p - 1$, p and $p + 1$. This difficulty has been overcome by using a further suggestion of Sells' (Ref. 1) for a more elaborate scheme which does not possess the inherent defect of inducing small residual discontinuities in chordwise slope as does the quadratic scheme. This is a cubic interpolation scheme which is a weighted average of a forward and a backward difference scheme of the type mentioned above. This has the effect of reducing the errors found previously to about 1 per cent and the time taken for a typical calculation is also reduced by about a quarter, since the more accurate definition of the interpolated values of $Q(B')$ reduces the degree of refinement necessary in the trapezoidal integration. The time reduction is more important when calculating the streamwise perturbation velocity component, since the singularity (chordwise) at the control point is 'stronger' than for the sidewash and hence requires a more precise numerical definition to achieve the same degree of accuracy for the final integral.

A special case arises when we wish to compute $u(x, 0, 0)$; and we must take care that the only information used comes from the starboard wing. For swept planforms, the source lines will be kinked at the centreline in the physical plane, and since we wish to preserve this feature, we make a parabolic interpolation between information at the centreline and the first and second outboard stations. G_1 and G_2 at the centreline may then be calculated from the first and second derivatives of the parabola there. We now have all the information necessary for a numerical chordwise integration of functions (102) and (107).

8. Examples

We now proceed to test all the features that have been incorporated in the programs whose structure has been described above. Firstly, in order to check the G_0 terms in our source function representation, a sheared wing of large aspect ratio was chosen, since G_1 and G_2 are identically zero in this case. With this test completed satisfactorily, the G_1 terms may be checked from calculations made on R.A.E. wing 'A' for which only G_2 is identically zero. A final test was made on a wing having linear planform taper and linear thickness taper for which our three-term Taylor expansion representation of the source function (24) is exact. Since we have established the accuracy of the G_0 and G_1 terms by this time, this last wing will test the G_2 terms.

Lastly a demonstration of the programs' function on a 'real' wing is given, together with comparative calculations using the method of Freestone and the R.A.E. standard method.

8.1. Sheared Wing of Large Aspect Ratio

The section shape was chosen to be

$$z_t = k\sqrt{\xi}(1 - \xi), \qquad 0 \leqslant \xi \leqslant 1 \tag{108}$$

and

$$\tau = \frac{t_{\max}}{c} = 0{\cdot}12$$

so that at the centre section, we have that

$$u(x, 0, 0) = \cos\Lambda\, S^{(1)}(x) - \frac{\cos\Lambda}{\pi} \ln\left\{\frac{1 + \sin\Lambda}{1 - \sin\Lambda}\right\} \frac{\partial z_t}{\partial x} \tag{109}$$

where

$$S^{(1)}(x) = \frac{0{\cdot}15589}{\pi} \int_0^1 \frac{1 - 3\xi}{2\sqrt{\xi}} \frac{d\xi}{x - \xi}, \tag{110}$$

$$\frac{\partial z_t}{\partial x} = 0{\cdot}15589\left(\frac{1 - 3\xi}{2\sqrt{\xi}}\right) \tag{111}$$

and

$$\Lambda = 45°. \tag{112}$$

Far from the centre section,

$$u(x, \infty, 0) = \cos \Lambda \, S^{(1)}(x). \tag{113}$$

A numerical experiment, using a 45 degree swept wing of aspect ratio 8, was run, and the results at the centre section ($y/s = 0$) and mid-semispan ($y/s = 0{\cdot}5$) are presented in Figs. 5 and 6 respectively. It is noted how closely the predictions of the $z = 0$ program agree with the velocities on the infinite wing derived from formulae (109) and (113). The $z = 0$ program was run using as data information from 20 chordwise partition lines and 4 spanwise partition lines. Where possible, the results for $z = 0$ were compared with calculations from Freestone's program (30 × 20 grid) and we see that the agreement is very good to within the limits of graphical accuracy (three figures). In addition, the program for $z \neq 0$ was also run at the same spanwise stations using $z = 0{\cdot}003$ and $0{\cdot}006$ and it is clear (again from Figs. 5 and 6) that the velocity distribution for $z = 0{\cdot}003$ lies midway between the distribution for $z = 0{\cdot}0$ and that for $z = 0{\cdot}006$, except very close to the leading edge. This increases our confidence in the consistency of the two programs since the variation of velocity for small z is known to be linear near the wing planform.

8.2. R.A.E. Wing 'A'

The next step involves testing the programs on wings for which only G_2 is identically zero. Wing 'A' (of Ref. 11) is an obvious choice. It has an aspect ratio of 6, planform taper ratio of 1/3, but no thickness taper. The section shape is the 9 per cent thick R.A.E. 101, which may be defined to reasonable accuracy by the analytic formula

$$\begin{aligned}\frac{z}{c} = (((((((&- 1{\cdot}496936\xi + 6{\cdot}36417)\xi - 10{\cdot}81622)\xi + 9{\cdot}14093)\xi - 3{\cdot}75674)\xi + \\ &+ 0{\cdot}551483)\xi + 0{\cdot}00886203)\xi + 0{\cdot}00444314)\xi + 0{\cdot}1112074\sqrt{\xi}(1 - \xi).\end{aligned} \tag{114}$$

For unit semispan, the leading edge and chord are given by

and

$$\left.\begin{aligned} x_l &= 0{\cdot}7440168\,Y \\ c &= 0{\cdot}5 - 0{\cdot}3333333\,Y \end{aligned}\right\} \tag{115}$$

where $0 \leqslant Y = y/s \leqslant 1$.

A comparison with Freestone's results has been made on the wing planform $z = 0$ at and near the root for both u and v. The three spanwise stations chosen were $\eta = 0$, $0{\cdot}04878$ and $0{\cdot}0976$ which result from Freestone's choice of grid 50 (chordwise) × 20 (spanwise) points, where the partitioning (spanwise) of the wing is chosen such that there are 20 whole panels on the half wing plus half of the panel 'covering' the centre section ($Y = 0{\cdot}04878 = 1/20{\cdot}5$). The results of the comparison are shown in Figs. 7 and 8. The agreement between the present method and Freestone's method is seen to be very good for $u(Y = 0)$ but there is a slight tendency for Freestone's results to oscillate about those of the present method.

In all these cases, the subsonic results have been obtained from the incompressible results by application of the Prandtl–Glauert rule whereas Freestone, by using the equations for compressible subsonic flow, retains a factor $\beta(= \sqrt{1 - M^2_\infty})$ throughout his computations which may lead to numerical differences with the present work for sufficiently high subsonic Mach numbers (and also involves more multiplications on the computer).

The $z \neq 0$ programs for v and w were also run at $M_\infty = 0$ and the results compared with those from the A. M. O. Smith program. Substantial differences between the present method and the method of A. M. O. Smith[6] occur since, in the latter method, the boundary conditions are applied on the wing surface, but in the present method they are taken on the wing planform. These discrepancies can be accounted for by second-order effects and estimates of the differences for both v and w are outlined in Appendix B and the results plotted in Figs. 9 and 10 for near mid-semispan stations, so chosen to minimize root and tip effects for a tapered planform.

8.3. Wings with Thickness and Planform Taper

In order to check the terms in (47), (54) and (55) involving the second spanwise coefficient G_2, a wing was devised having both linear planform taper and linear thickness taper across the span. Thus the source function $Q \sin \phi$ possesses a quadratic variation with η, and the parabolic fitting described in Section 7 will be exact.

The leading and trailing edges of the wing planform are given by

$$\left.\begin{aligned} x_l &= 1{\cdot}1875Y \\ x_t &= 0{\cdot}5 + 0{\cdot}8125Y \end{aligned}\right\} \qquad Y = y/s, \qquad 0 \leqslant Y \leqslant 1 \tag{116}$$

and the coordinates of the upper surface are given by

$$\frac{z}{c(Y)} = 0{\cdot}1\sqrt{\xi}(1 - \xi)(1 - Y). \tag{117}$$

The programs for $z = 0$ and $z \neq 0$ were run at three different spanwise stations $\eta = 0{\cdot}0$, $0{\cdot}1$ and $0{\cdot}5$ using a 23×4 grid; the comparisons with the results of Freestone's program ($z = 0$ only) using a 40×40 mesh are shown in Fig. 11. The consistency of the values of u on $z = 0$ with linearly extrapolated values for small z is shown in Tables A1, A2 and A3, given in Appendix A.

As a demonstration of the programs' operation in computing u on a 'real' wing, we choose a wing based on the wing 'A' planform and R.A.E. (N.P.L.) 5212 section but with some modification in the vicinity of the root so as to maintain a reasonably uniform isobar sweep pattern close to the centre section. The root section thickness distribution is sketched in Fig. 12, and an analytic formula which closely approximates this is

$$\frac{z}{c} = \cos 30^\circ \left(a_0\sqrt{\xi}(1 - \xi) + \sum_{k=1}^{8} a_k \xi^k \right) + 0{\cdot}15\sqrt{\xi}(1 - \xi)^2(0{\cdot}336 - \xi)\frac{1}{2}\left(1 + \cos \pi \frac{Y}{Y_1}\right) +$$

$$+ 0{\cdot}06\sqrt{\xi}(1 - \xi)\frac{1}{2}\left(1 + \cos \pi \frac{Y}{Y_2}\right), \tag{118}$$

where the second term is included only when

$$|Y| \leqslant Y_1 = 0{\cdot}10$$

and the third term is included only when

$$|Y| \leqslant Y_2 = 0{\cdot}075;$$

also

$$\begin{aligned} a_0 &= 0{\cdot}18022, \\ a_1 &= -0{\cdot}133906, \\ a_2 &= 0{\cdot}734305, \\ a_3 &= -3{\cdot}272930, \\ a_4 &= 12{\cdot}417360, \\ a_5 &= -29{\cdot}201795, \\ a_6 &= 37{\cdot}501670, \\ a_7 &= -24{\cdot}255895 \end{aligned}$$

and

$$a_8 = \quad 6{\cdot}211191.$$

The distributions of streamwash in the root, near-root and mid-semispan positions are shown in Figs. 13, 14 and 15 together with the predictions of the Freestone method and the R.A.E. standard method.* As we would expect, the best agreement between the three methods occurs near mid-semispan where root and tip effects are least appreciable, whilst nearer to the root, the R.A.E. standard method predicts a much more rapid fall in the values of u near the leading edge than does the present method, which is in close proximity to the Freestone results. However, at the root station itself ($Y = 0$), the Freestone method clearly predicts the wrong trend near the leading edge but is in quite good agreement elsewhere. In this case, the R.A.E. standard method copes quite well with the situation and predicts the expected trend towards the leading edge and is fairly closely allied with the other two methods over the rest of the chord.

8.4. Computation Times and Storage Requirements

Throughout the numerical experiments described herein, an ICL 1907 computer was used and the calculation times quoted refer to this machine alone. If we consider a typical case of computing u, v and w for a swept wing with uniform aerofoil section, using a grid of 20 chordwise partitions by 10 spanwise, the time taken to calculate u to an accuracy of three significant figures would be 3 seconds and for v and w about 2·5 seconds each. The reason for this is that the integrals in the formulae for v and w have less strong numerical chordwise singularities than that for u and hence they do not require such a high level of chordwise refinement to achieve the same degree of accuracy.

If the number of partitions across the span is doubled then the computation time per point is doubled; however, this is not quite true for the same increase in datum points on a given chord line, for which the time increases to about 2·2 times the old time.

The storage requirements of all the programs is very modest and well within the capacity of a small machine like the ICL 1907. For example, to compute all the velocity components on wing 'A' using a 23×23 grid would require 16K variables or 32K words of storage. No additional disc space is required.

9. Concluding Remarks

A method has been developed for computing the three components of perturbation velocity induced by a planar source distribution which represents a thick wing at zero incidence, both on and off the wing planform. In this respect, the method holds an advantage over Freestone's pioneer program, which is tailored to calculations on $z = 0$. In addition, some increase in accuracy or saving of time required to achieve a given accuracy is claimed. Generally speaking, where direct comparisons are possible, Freestone's velocity distribution curves tend to oscillate slightly about the inherently smoother curves produced by the present method. As has been remarked previously (and in Ref. 1) this may be due to the fixed number of grid refinements employed and the lack of tailoring of the coordinate system to the wing planform which may produce errors near the edges especially at stations outboard of $Y = 0{\cdot}4$, say, on swept, tapered planforms. The present method does not meet with these difficulties.

The numerical techniques used are broadly those developed by Sells[1] for the computation of downwash due to a given doublet distribution, and enable an 'exact' treatment of the case $u(x, 0, 0)$ to be attempted, although the solution will be singular as $x \to 0$ (*i.e.* at the wing apex).

In the problem of designing wing-body combinations for a given load distribution and thickness distribution, the present method should provide a valuable tool not only because of its efficiency but also on account of its compatibility with the method of Ref. 1.

* The formula for evaluating u according to the R.A.E. standard method is the one described in Ref. 14 with Λ_t being interpreted as the geometric sweep.

LIST OF SYMBOLS

a	Local sweep $x_l' + c'\xi$
b	$\sqrt{(a^2 + 1)}$
$c, c(y')$	Chord
c'	$dc(y)/dy$
E, E'	Coefficients in the expansion of Q about the reference line (*see* Section 7.1)
G_0, G_1, G_2	Coefficients in the three term Taylor expansion about the control line of Q; $Q = G_0(\phi) + \eta^2 G_2(\phi)$
h	$x' - x = h + \eta a$
I	Indefinite integral over one spanwise strip (*see* equations (24))
J_0, J_1, J_2	$I = G_0 J_0 + G_1 J_1 + G_2 J_2$
M_∞	Free stream Mach number
p	Point of chordwise subdivision
$q^{(1)}$	First-order source function $2\,\partial z_t(x, y)/\partial x$
$q^{(2)}$	Second-order source function
Q	$q(x, y)c(y) \sin\phi$
r	$r^2 = (x' - x)^2 + (y' - y)^2 + z^2$ $= (h + \eta a)^2 + \eta^2 + z^2$
s	Semispan (usually unity)
U_∞	Free stream velocity
u, v, w	Components of perturbation velocity (u = streamwash, v = sidewash, w = upwash)
x, y, z	Cartesian coordinates of the control point
x', y'	Cartesian coordinates of a point in the wing plane
x_l	Coordinate of the leading edge
Y	Coordinate normalised with respect to semispan ($= y/s$)
β	$\sqrt{(1 - M_\infty^2)}$
Δ	$a(\partial I/\partial h) - \partial I/\partial\eta$
η	$y' - y$; spanwise coordinate measured from the control line
η_+, η_-	Limits of spanwise integration strip
η^*	Reference point of expansion; $\eta_- \leqslant \eta^* \leqslant \eta_+$
ϑ	$G_0(\phi)\left[\dfrac{\eta}{r_0}\right]_{\eta_-}^{\eta_+}$ (*see* equation (64))
Λ_x, Λ_ξ	Local sweep angle at x, ξ
ξ	Local section coordinate; $x' = x_l(y') + \xi c(y')$
ϕ	Chordwise coordinate; $x' = x_l(y') + \frac{1}{2}(1 - \cos\phi)c(y')$
Φ	Velocity potential
χ	$-\partial I/\partial h$

Subscripts

0	First subscript on r, or second subscript on I, values when $z = 0$

1	First subscript on r, value when $\eta = 0$
c	Values when $h = 0$ (control point)
l	Leading edge
s	Quantities whose direction is perpendicular to leading edge
t	Thickness coordinate
∞	Free stream conditions at upstream infinity

REFERENCES

No.	*Author(s)*	*Title, etc.*
1	C. C. L. Sells	Calculation of the induced downwash field on and off the wing plane for a swept wing with given load distribution. A.R.C. R.& M. 3725 (1969).
2	M. M. Freestone	Numerical evaluation of singular integrals of linearised subsonic wing theory. A.R.C. 29729 (1967).
3	M. M. Freestone	An approach to the design of the thickness distribution near the centre of an isolated swept wing at subsonic speed. A.G.A.R.D. Conference Proceedings No. 35, Paper 15 (1968).
4	B. Thwaites	*Incompressible aerodynamics.* Chapter VII. Clarendon Press (1960).
5	R. C. Lock	A note on subsonic linearised theory for symmetrical cranked wings at zero-incidence. N.P.L. Aero. Note 1090 (A.R.C. 32225) (1970).
6	J. L. Hess and A. M. O. Smith ..	*Calculation of potential flow about arbitrary bodies.* Progress in Aeronautical Sciences, Vol. 8. Ed. D. Küchemann, Pergamon Press (1967).
7	R. C. Lock	Revised compressibility corrections in subsonic swept wing theory, with applications to wing design. N.P.L. Aero. Memo. No. 64 (A.R.C. 31310) (1969).
8	D. Küchemann	Some remarks on the interference between a swept wing and a fuselage. R.A.E. Technical Report 70093 A.R.C. 32307 (1970).
9	J. Weber	Second-order small perturbation theory for finite wings in incompressible flow. R.A.E. Technical Report 72171 A.R.C. 34 469 (1972).
10	J. Weber and M. G. Joyce	Interference problems on wing fuselage combinations: Part II Symmetrical upswept wing at zero incidence attached to a cylindrical fuselage at zero incidence in midwing position. R.A.E. Technical Report 71179 A.R.C. 33437 (1971).
11	D. A. Treadgold and A. F. Jones ..	An outline of the research program on swept wings in the R.A.E. 8 ft × 6 ft transonic wind tunnel. R.A.E. Technical Memorandum Aero 1282 A.R.C. 32825 (1971).
12	R. C. Lock	Transonic Aerodynamics Course, City University (1970).
13	J. Weber	The calculation of the pressure distribution over the surface of two-dimensional and swept wings with symmetrical aerofoil sections. R. & M. 2918 (1953).
14	—	Method for predicting the pressure distribution on swept wings with subsonic attached flow. *T.D.M. 6312, Roy. Aero. Soc.* (1963).

APPENDIX A

Comparative Values of u on and off the Planform of a Tapered Wing

Table A1

$y/s = 0$

ξ	$z = 0$ (computed)	$z = 0$ (linear extrapolation)	$z = 0{\cdot}0015$	$z = 0{\cdot}003$
0·0185	−0·0585	−0·0597	−0·0870	−0·1143
0·0728	0·0250	0·0257	0·0206	0·0155
0·1587	0·0504	0·0509	0·0490	0·0471
0·2700	0·0604	0·0609	0·0599	0·0589
0·3983	0·0629	0·0629	0·0622	0·0615
0·5341	0·0598	0·0596	0·0591	0·0586
0·6674	0·0521	0·0521	0·0517	0·0513
0·7883	0·0400	0·0400	0·0397	0·0394
0·8879	0·0225	0·0225	0·0222	0·0219

Table A2

$y/s = 0{\cdot}1$

ξ	$z = 0$ (computed)	$z = 0$ (linear extrapolation)	$z = 0{\cdot}0015$	$z = 0{\cdot}003$
0·0185	0·0745	0·0681	0·0452	0·0223
0·0728	0·0732	0·0730	0·0686	0·0642
0·1587	0·0710	0·0707	0·0692	0·0675
0·2700	0·0672	0·0669	0·0660	0·0651
0·3983	0·0608	0·0606	0·0600	0·0594
0·5341	0·0513	0·0511	0·0507	0·0503
0·6674	0·0379	0·0378	0·0374	0·0370
0·7883	0·0197	0·0197	0·0194	0·0191
0·8879	−0·0027	−0·0027	−0·0027	−0·0027

Table A3

$y/s = 0{\cdot}5$

ξ	$z = 0$ (computed)	$z = 0$ (linear extrapolation)	$z = 0{\cdot}0015$	$z = 0{\cdot}003$
0·0185	0·0481	0·0391	0·0249	0·0107
0·0728	0·0458	0·0454	0·0419	0·0384
0·1587	0·0422	0·0417	0·0405	0·0392
0·2700	0·0372	0·0370	0·0363	0·0356
0·3983	0·0311	0·0309	0·0304	0·0299
0·5341	0·0238	0·0238	0·0234	0·0230
0·6674	0·0156	0·0156	0·0152	0·0148
0·7883	0·0061	0·0061	0·0058	0·0055
0·8879	−0·0053	−0·0052	−0·0053	−0·0054

APPENDIX B

Second-Order Effects

The differences between the present method and the A. M. O. Smith method for computing velocity components on the wing surface may be accounted for by second-order effects. Near the mid-semispan we may attempt an analytic estimate (on wing 'A') and by way of example we choose the cases:

$$\Delta w = w_2 - w_1$$

and

$$\Delta v = v_2 - v_1$$

where the suffix 2 refers to the A. M. O. Smith calculation and 1 refers to the present method.

Now, for the upwash calculation, we may write

$$\begin{aligned} \Delta w &= w(q^{(2)}; x, y, z) - w(q^{(1)}; x, y, z) \\ &= w(q^{(1)} + \Delta q; x, y, z) - w(q^{(1)}; x, y, z) \\ &= w(\Delta q; x, y, z) \\ &\simeq w(\Delta q; x, y, 0) + O(\tau^3) \\ &\simeq \tfrac{1}{2}\Delta q(x, y). \end{aligned} \tag{B-1}$$

We would now like to express $\Delta q(x, y)$ in terms of the tabulated function $S^{(1)}(x)$. Using the results of Ref. 9 or Ref. 12

$$\Delta w = \tfrac{1}{2}\Delta q(x, y) = \frac{\partial}{\partial x}(z_t u^{(1)}) + \frac{\partial}{\partial y}(z_t v^{(1)}), \tag{B-2}$$

which is obtained from the second-order boundary condition together with the equation of continuity. Near the mid-semispan, root and tip effects will be minimal, so we may write

$$u^{(1)} \simeq S^{(1)} \cos \Lambda \tag{B-3}$$

and

$$v^{(1)} \simeq -S^{(1)} \sin \Lambda \tag{B-4}$$

where Λ = mid-chord sweep.

Inserting (B-3) and (B-4) in (B-2), we obtain

$$\Delta w = \cos \Lambda \frac{\partial}{\partial x}(z_t S^{(1)}(X)) - \sin \Lambda \frac{\partial}{\partial y}(z_t S^{(1)}(X)) \tag{B-5}$$

where

$$z_t = c(y) f(X) \tag{B-6}$$

and

$$X = \frac{x - x_t(y)}{c(y)}, \tag{B-7}$$

so that $f(X)$ is the section thickness normalised with respect to the local chord. Hence we find that

$$\frac{\partial X}{\partial y} = -\frac{1}{c(y)} \tan \Lambda, \qquad \frac{\partial z_t}{\partial x} = f'(X) \tag{B-8}$$

and

$$\frac{\partial z_t}{\partial y} = \frac{dc}{dy} f(X) - f'(X) \tan \Lambda.$$

Inserting expressions (B-8) into (B-5) and neglecting taper effects, we find that

$$\Delta w = \sec \Lambda \frac{d}{dx}(f(X)S^{(1)}(X)) \tag{B-9}$$

so that

$$\Delta v = -\tan \Lambda S^{(1)}[f(X)S^{(1)}(X)] \tag{B-10}$$

using the second-order source distribution.

Evaluating (B-9) for a 9 per cent thick R.A.E. 101 section using the values of $S^{(1)}(X)$ given in Ref. 13 for example, we obtain the following:

X	$S^{(1)}(X)$	$z_t(X)$	$S^{(1)}(X)z_t(X)$	$\frac{d}{dX}[S^{(1)}(X)z_t(X)]$ from graph of $sz_t : X$	$\sec \Lambda \frac{d}{dX}$ $[S^{(1)}(X)z_t(X)]$ (B-9)	Δw estimate from Fig. 9
0·9619	−0·0503	0·0031	−0·00015	+0·0000	+0·0000	+0·0000
0·8536	−0·0072	0·0118	−0·00008	−0·0004	−0·0046	−0·0045
0·6913	+0·0329	0·0248	+0·00082	−0·0086	−0·0065	−0·0070
0·5000	0·0819	0·0384	0·0031	−0·0140	−0·0162	−0·0160
0·3087	0·1302	0·0450	0·0059	−0·0054	−0·0062	−0·005
0·1464	0·1332	0·0377	0·0050	+0·0143	+0·0165	+0·0160
0·0381	0·1333	0·0211	0·0028	0·0276	0·0319	0·040

Inspection of the last two columns of the above table gives us confidence in the accuracy of our method based on the first-order source distribution which together with suitable second-order corrections is in quite good agreement with the nominally exact method of A. M. O. Smith. The results near the mid-semispan are plotted in Fig. 9.

We now evaluate (B-10) making use of the formula[13]

$$S^{(1)}[S_\nu^{(1)}(x)f_\nu(x)] = \sum_{\mu=1}^{N-1} s_{\mu\nu}^{(1)} S_\mu^{(1)}(x) f_\mu(x). \tag{B-11}$$

The sum on the right hand side of (B-11) can be evaluated from tables using $N = 8$ (Ref. 13) which was regarded as giving sufficient accuracy for the purpose of this demonstration. The following table and Fig. 11 show that the present method together with correction formula (B-10) correlates well with A. M. O. Smith computations.

X	$S^{(1)}(X)z_t(X)$	$S^{(1)}[S^{(1)}(X)z_t(X)]$	$-\tan \Lambda S^{(1)}[S^{(1)}(X)z_t(X)]$ (B-10)	Δv estimate from Fig. 10
0·9619	−0·00015	−0·0094	0·0054	0·004
0·8536	−0·00008	−0·0064	0·0037	0·003
0·6913	+0·00082	−0·0047	+0·0027	+0·0025
0·5000	0·0031	+0·0030	−0·0017	−0·002
0·3087	0·0059	0·0237	−0·0137	−0·013
0·1464	0·0050	0·0190	−0·0109	−0·0110
0·0381	0·0028	0·0191	−0·0110	−0·008

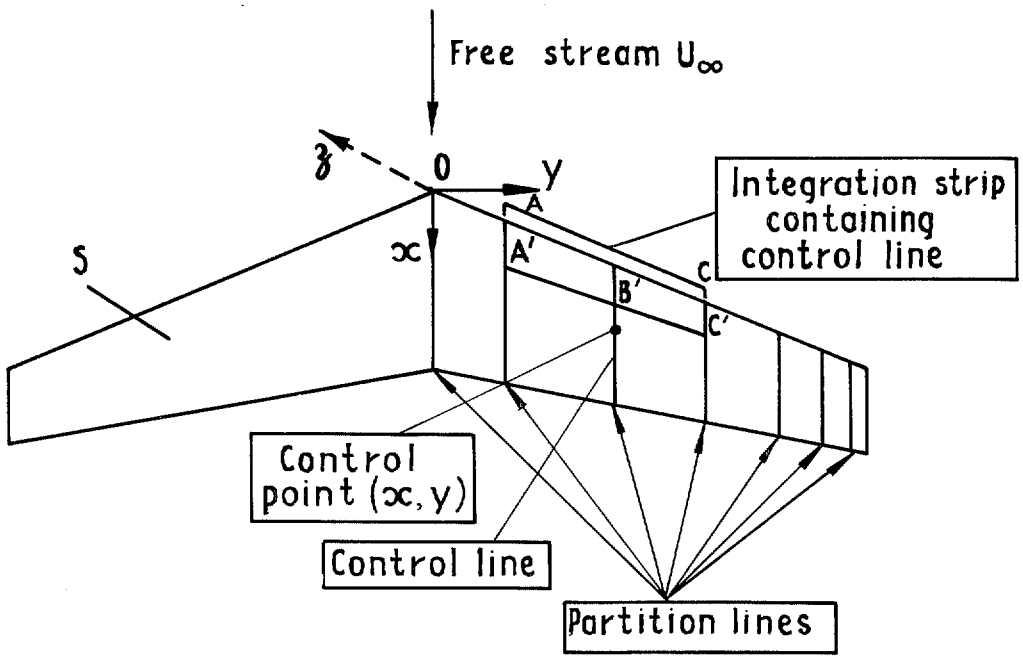

FIG. 1. Spanwise partitioning of wing.

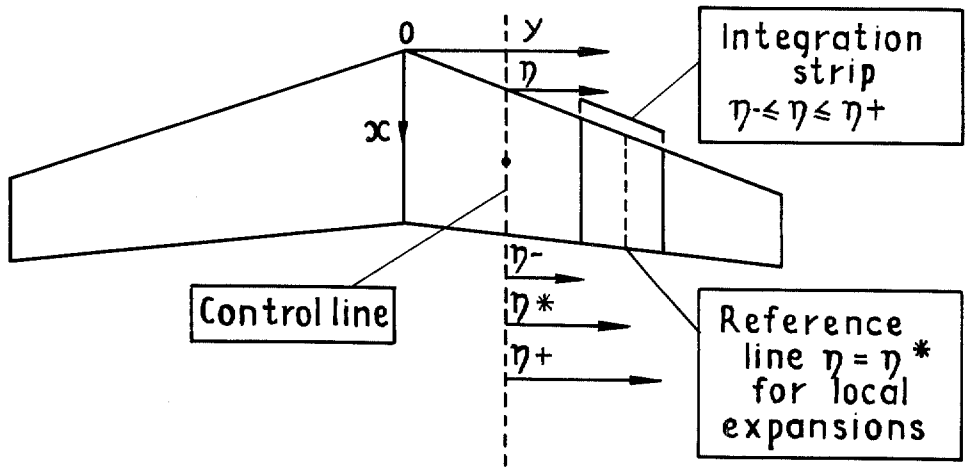

FIG. 2. Spanwise coordinate system relative to the control line.

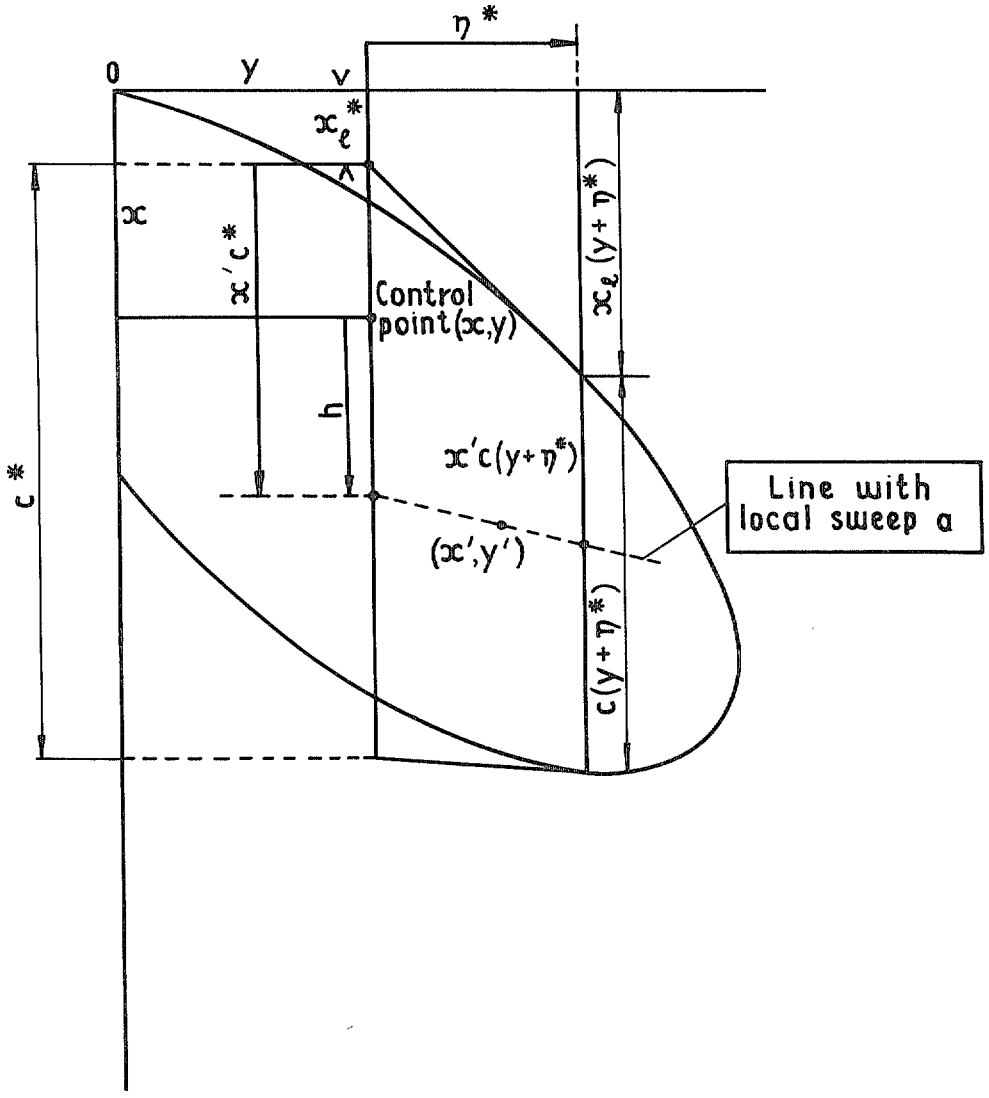

FIG. 3. Physical meaning of x_l^*, c^* and h.

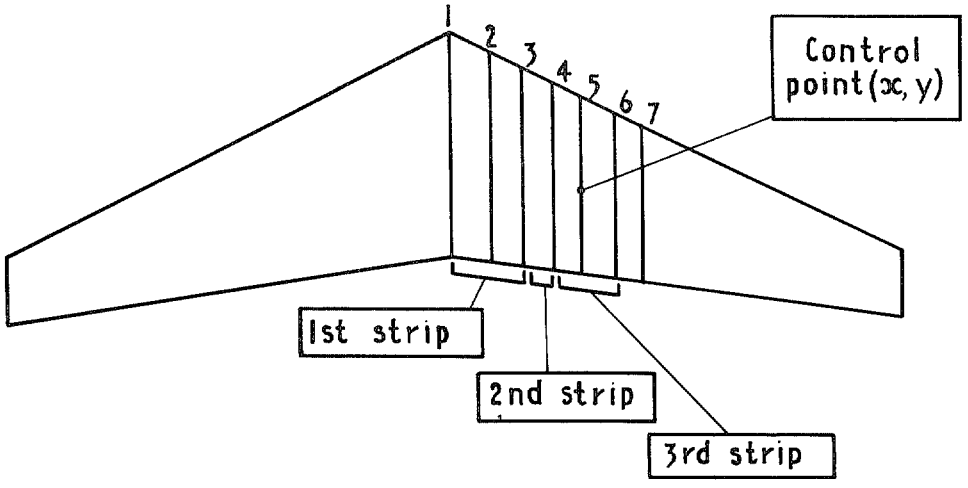

FIG. 4. Choice of integration strips relative to centreline and control line.

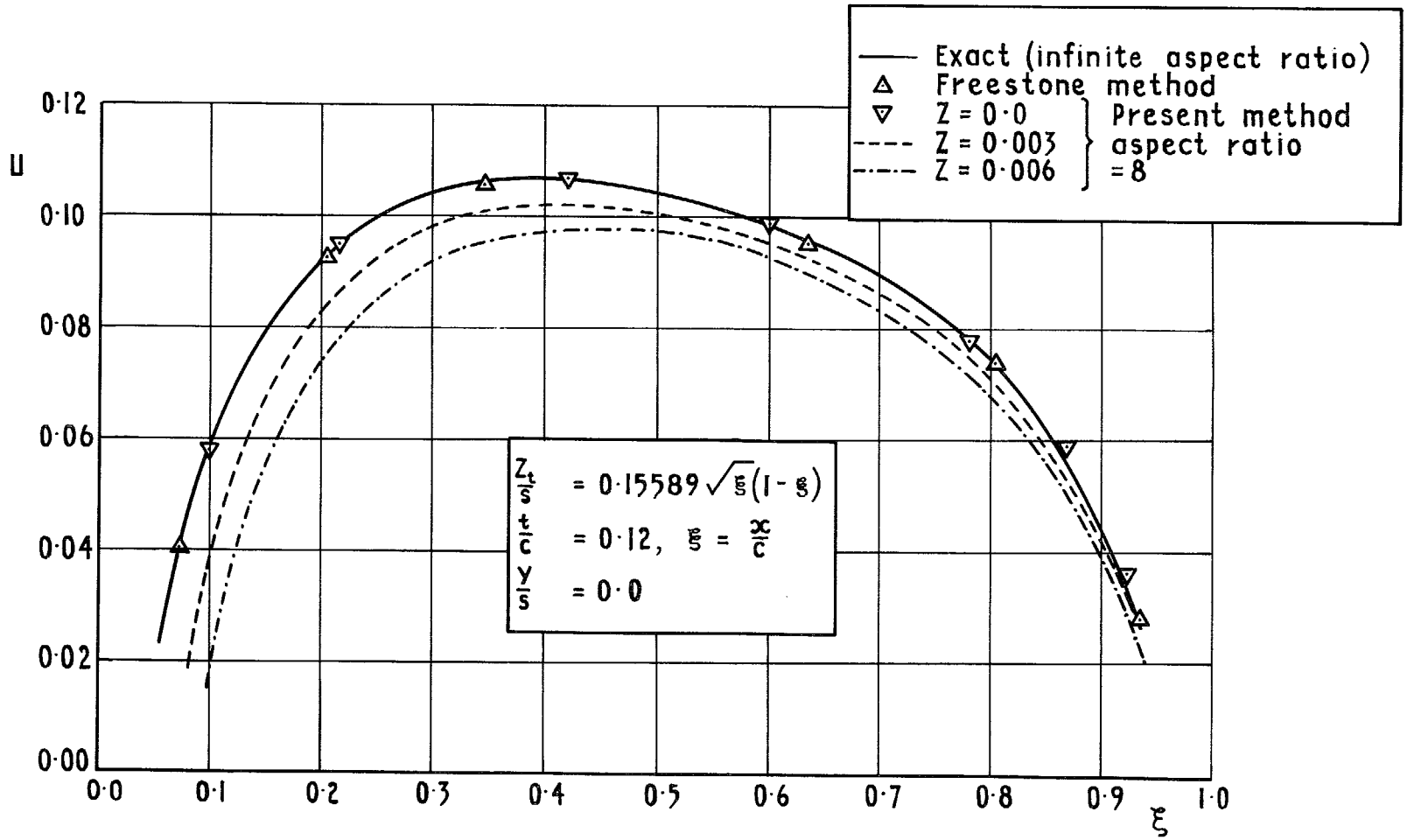

FIG. 5. Perturbation streamwash at the root of a constant chord 45° swept wing of aspect ratio 8.

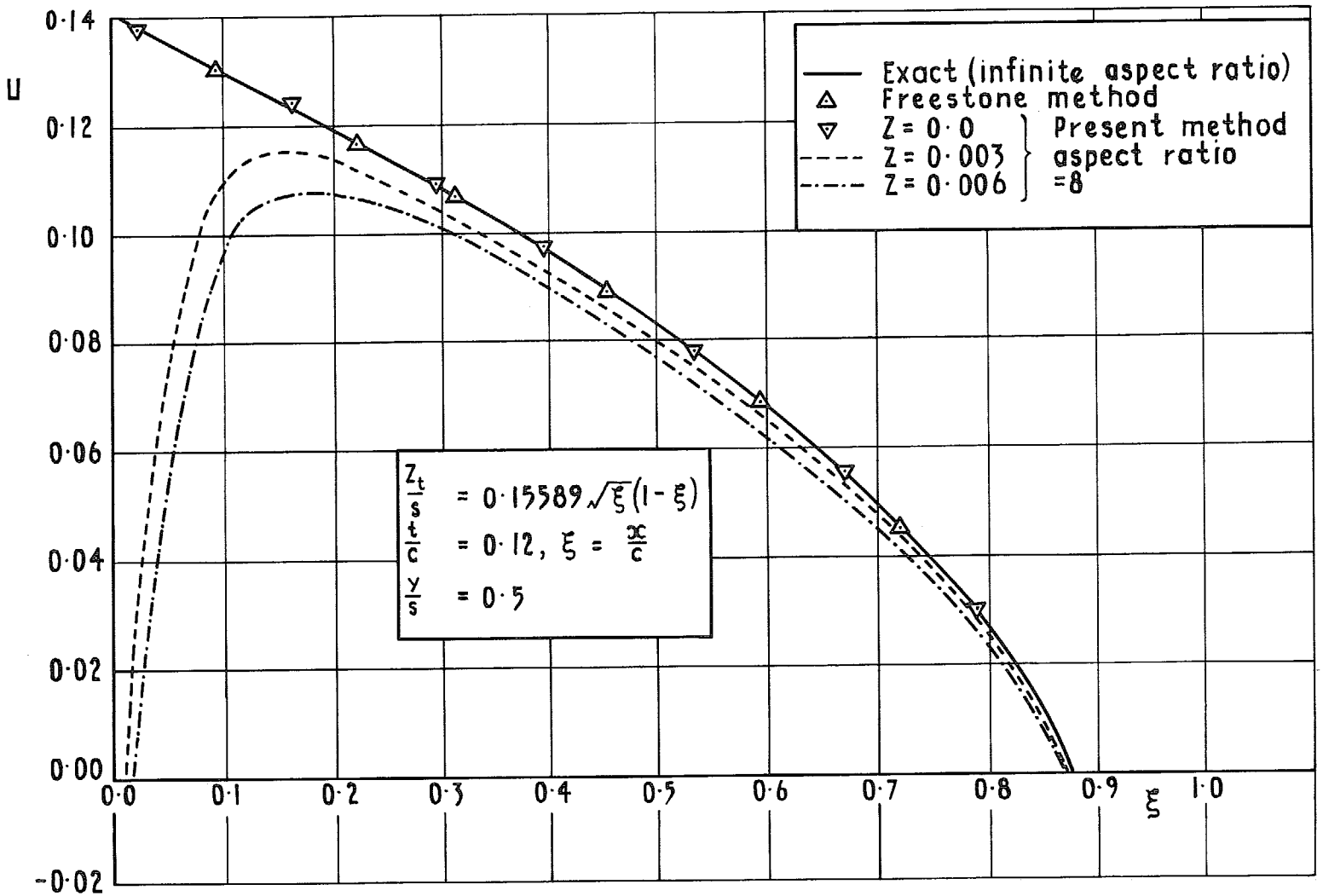

FIG. 6. Perturbation streamwash at the mid-semispan station for a constant chord 45° swept wing of aspect ratio 8.

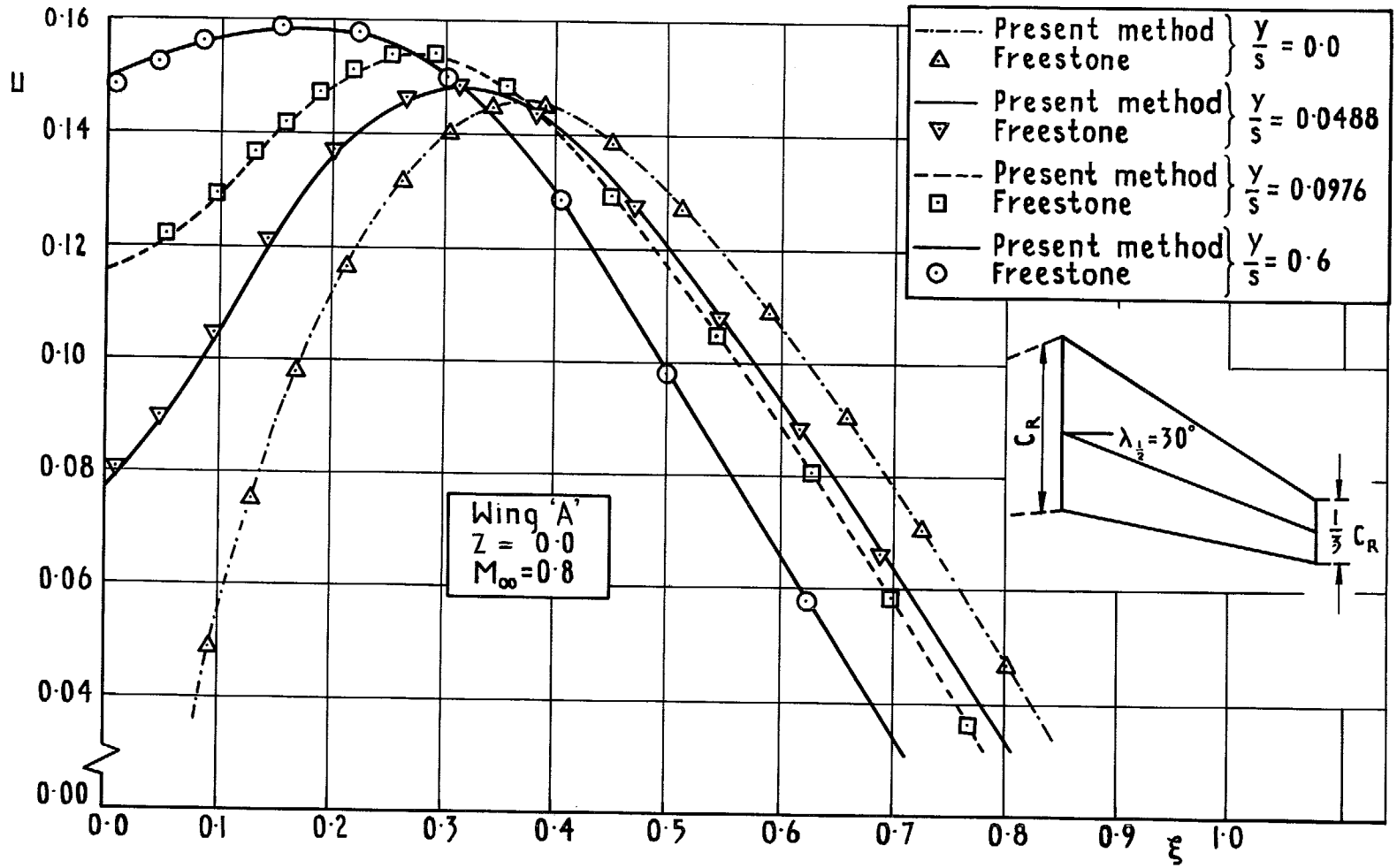

FIG. 7. Perturbation streamwash at and near the root of wing 'A' in a flow with free stream Mach number 0·8.

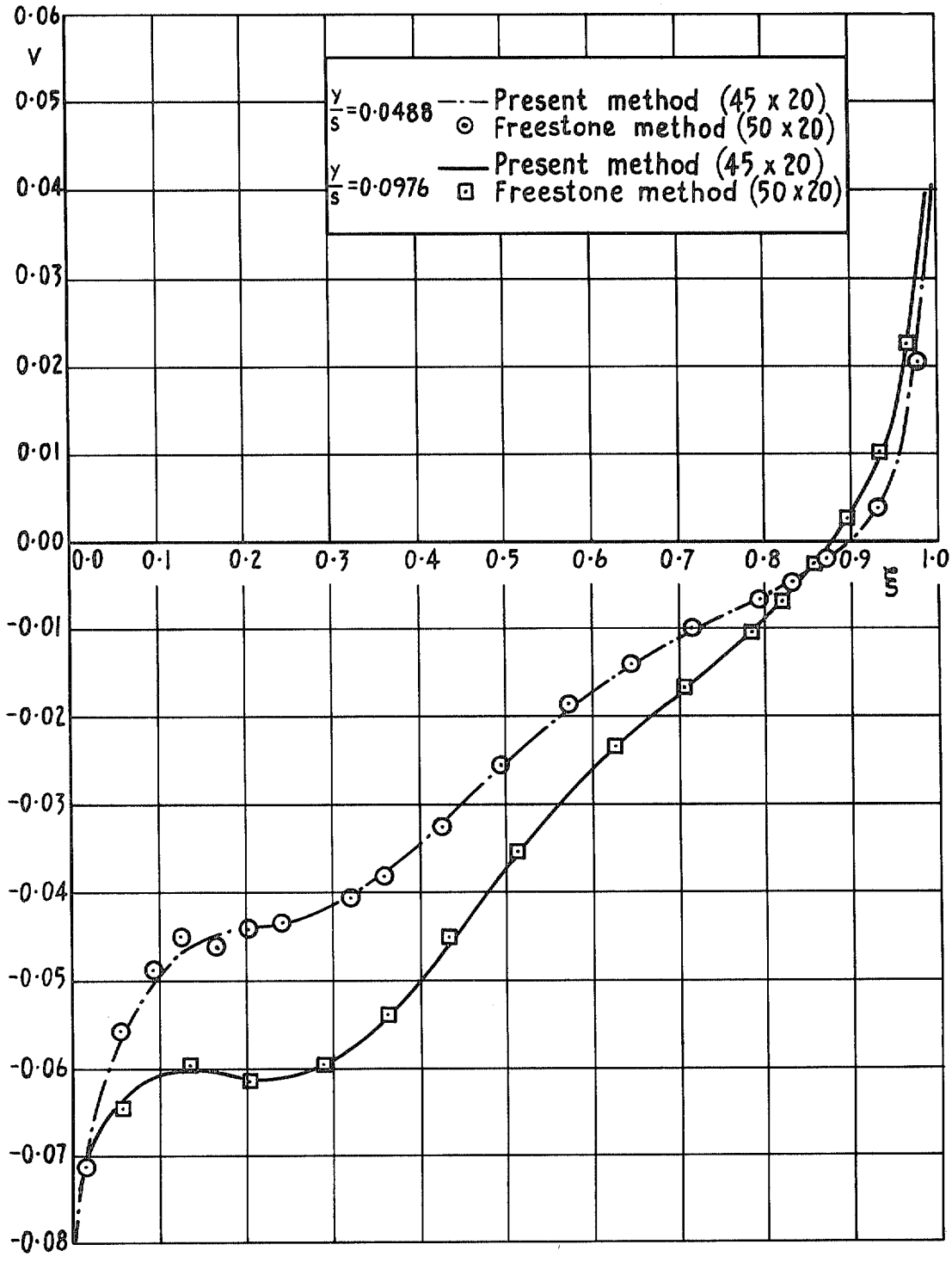

FIG. 8. Distribution of sidewash velocity component near the root of wing 'A' at $M_\infty = 0{\cdot}8$ on $Z = 0$

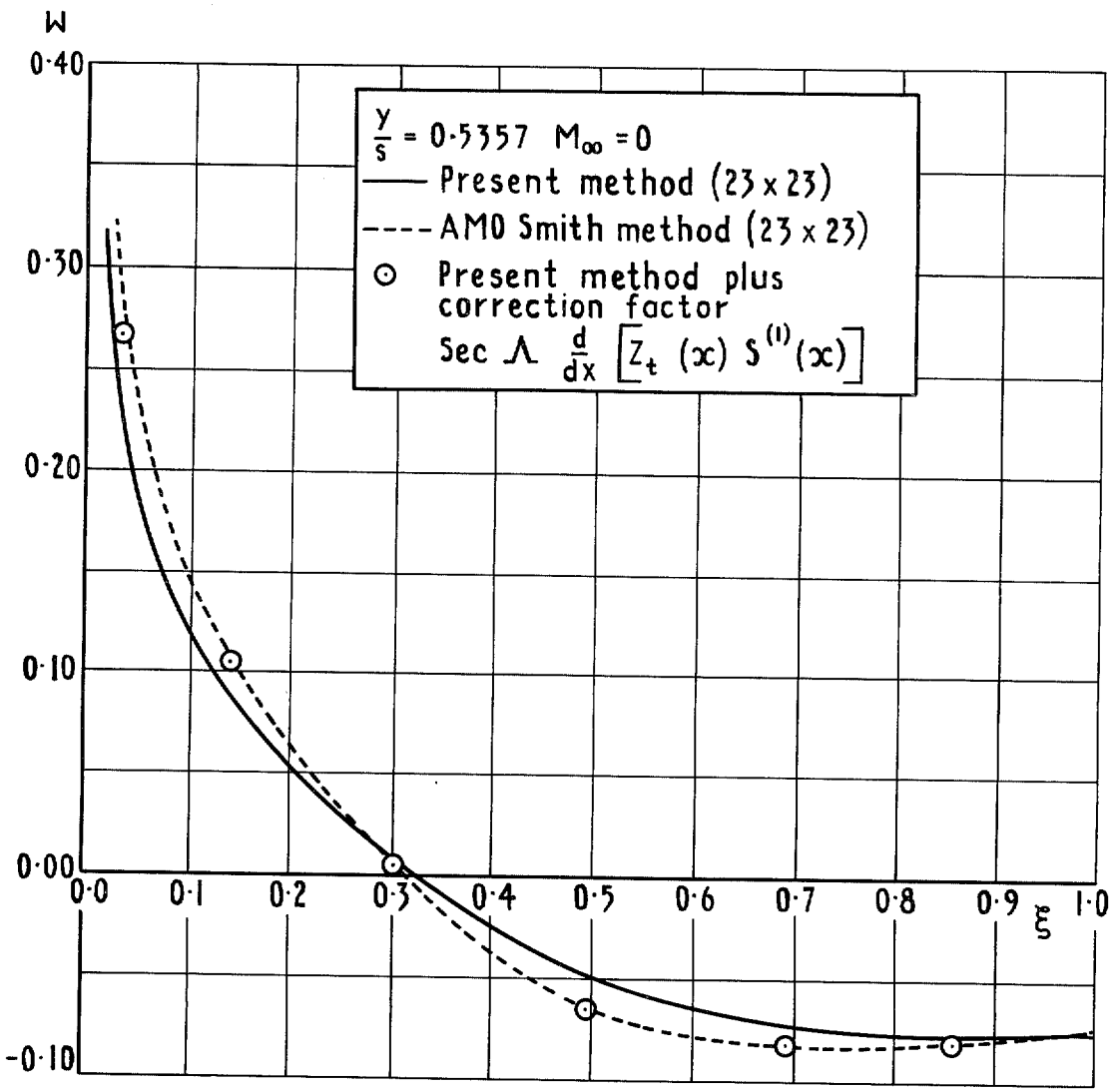

FIG. 9. Distribution of upwash velocity on the surface of wing 'A' near mid-semispan.

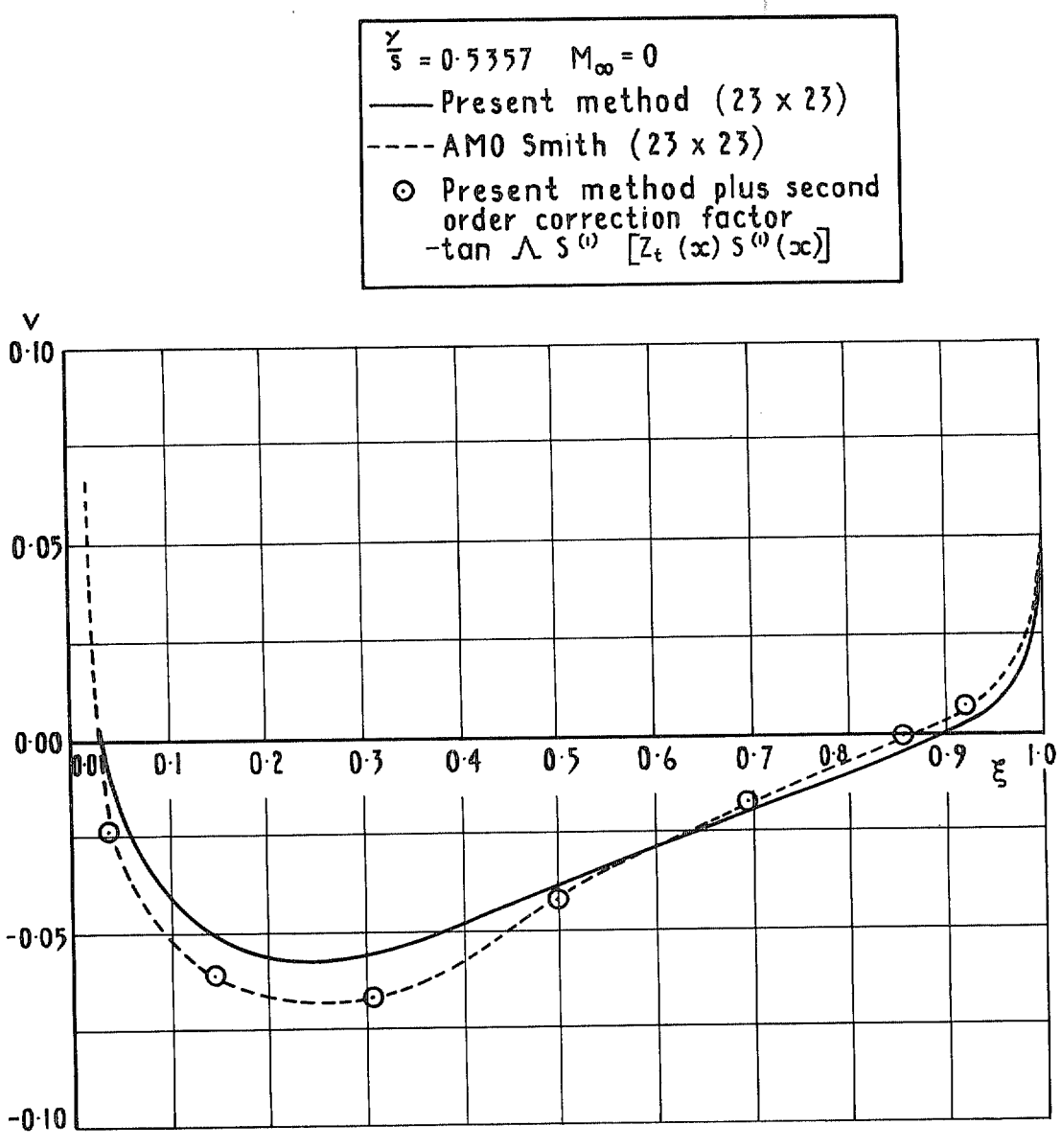

FIG. 10. Distribution of sidewash velocity on the surface of wing 'A' near mid-semispan.

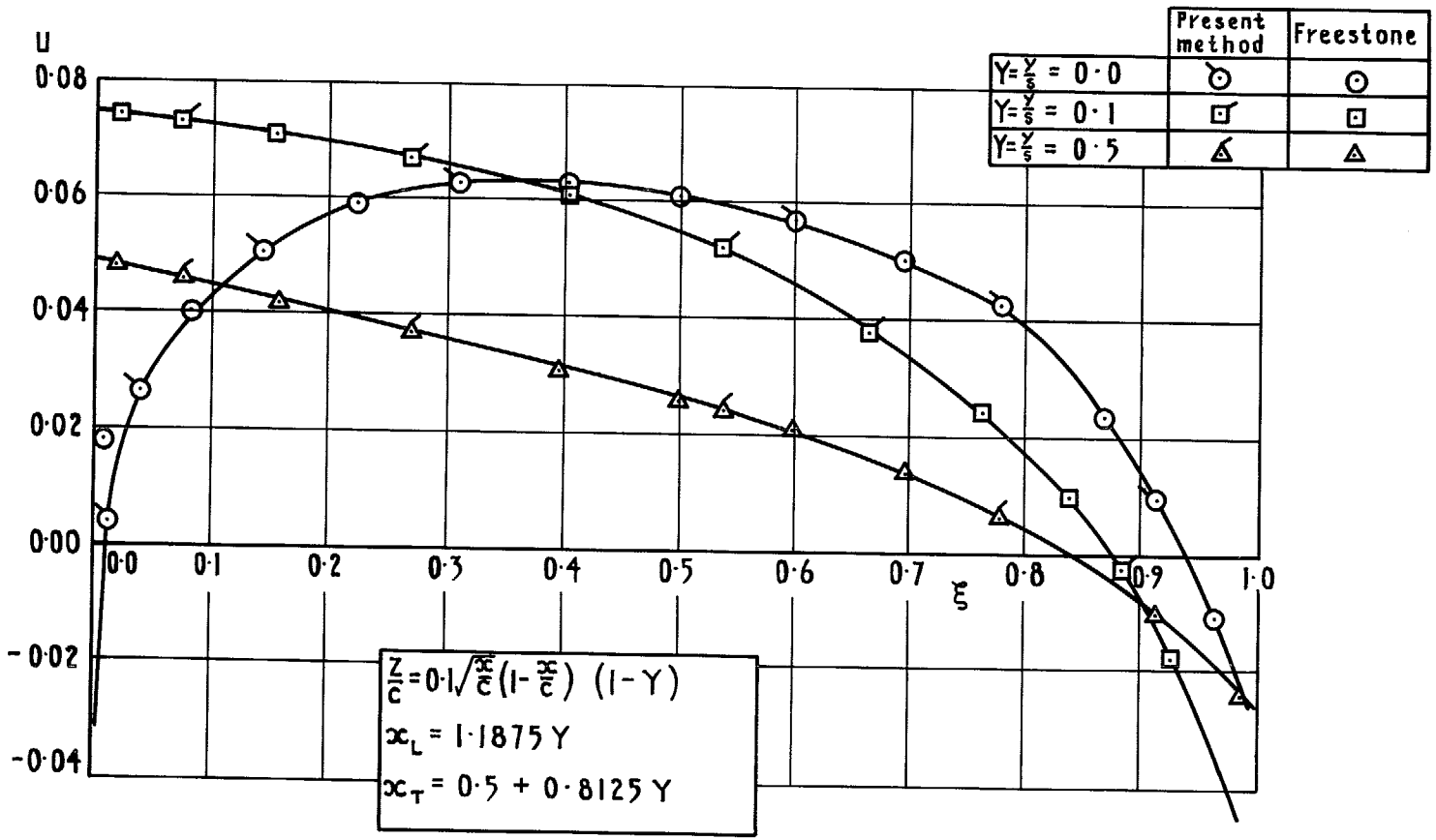

FIG. 11. Streamwise velocity distributions on a wing with 45° mid chord sweep, taper ratio $\frac{1}{4}$ and linear thickness taper.

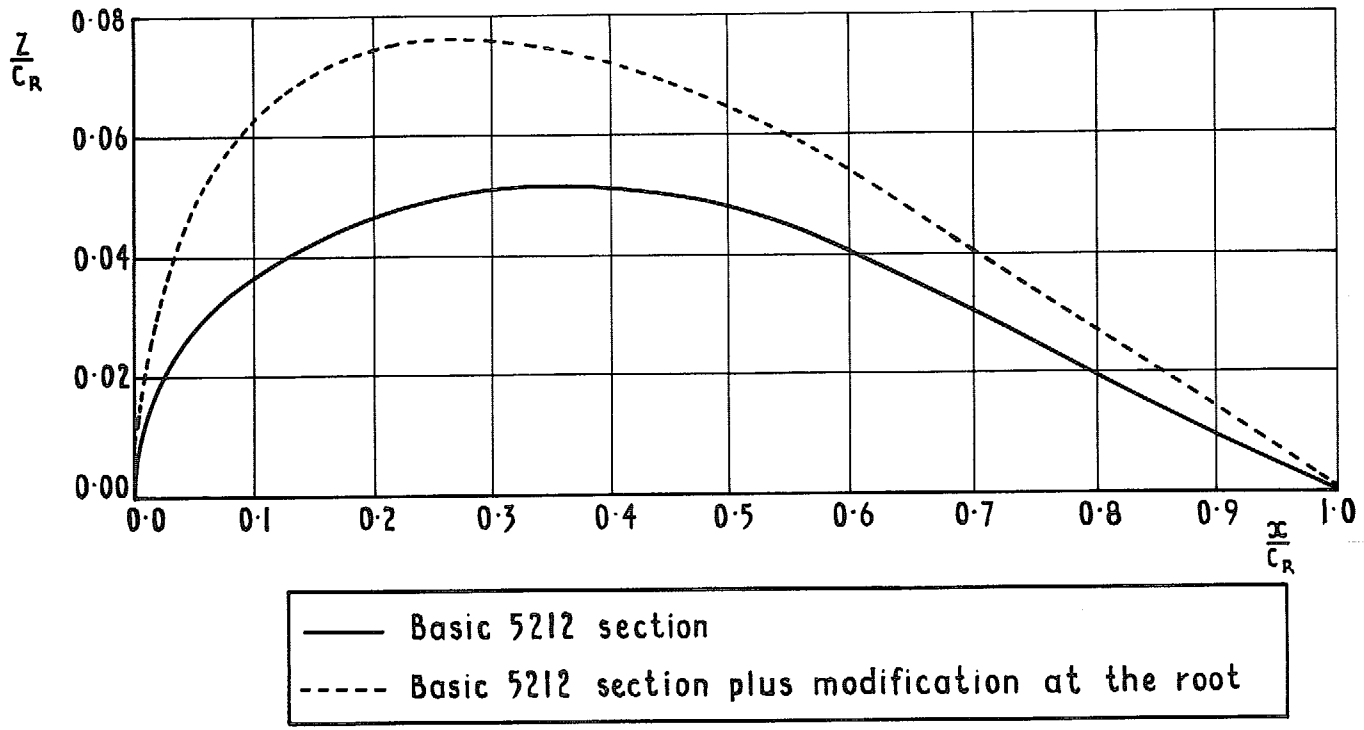

FIG. 12. Thickness distribution for R.A.E. (N.P.L.) 5212 modified wing.

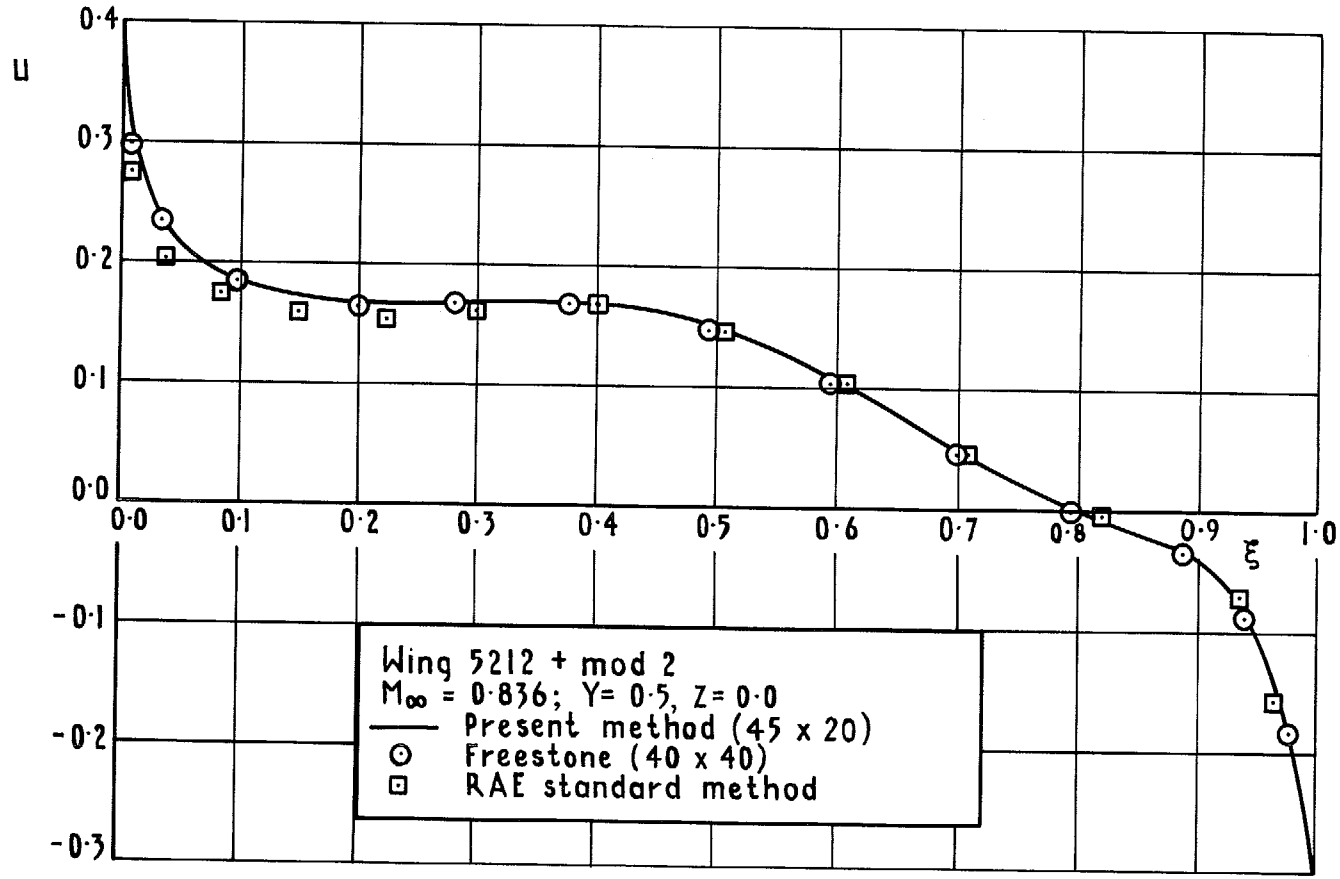

FIG. 13. Streamwise distribution of velocity on a wing with wing 'A' planform and R.A.E. (N.P.L.) 5212 section shape but modified in root region: mid-semispan station.

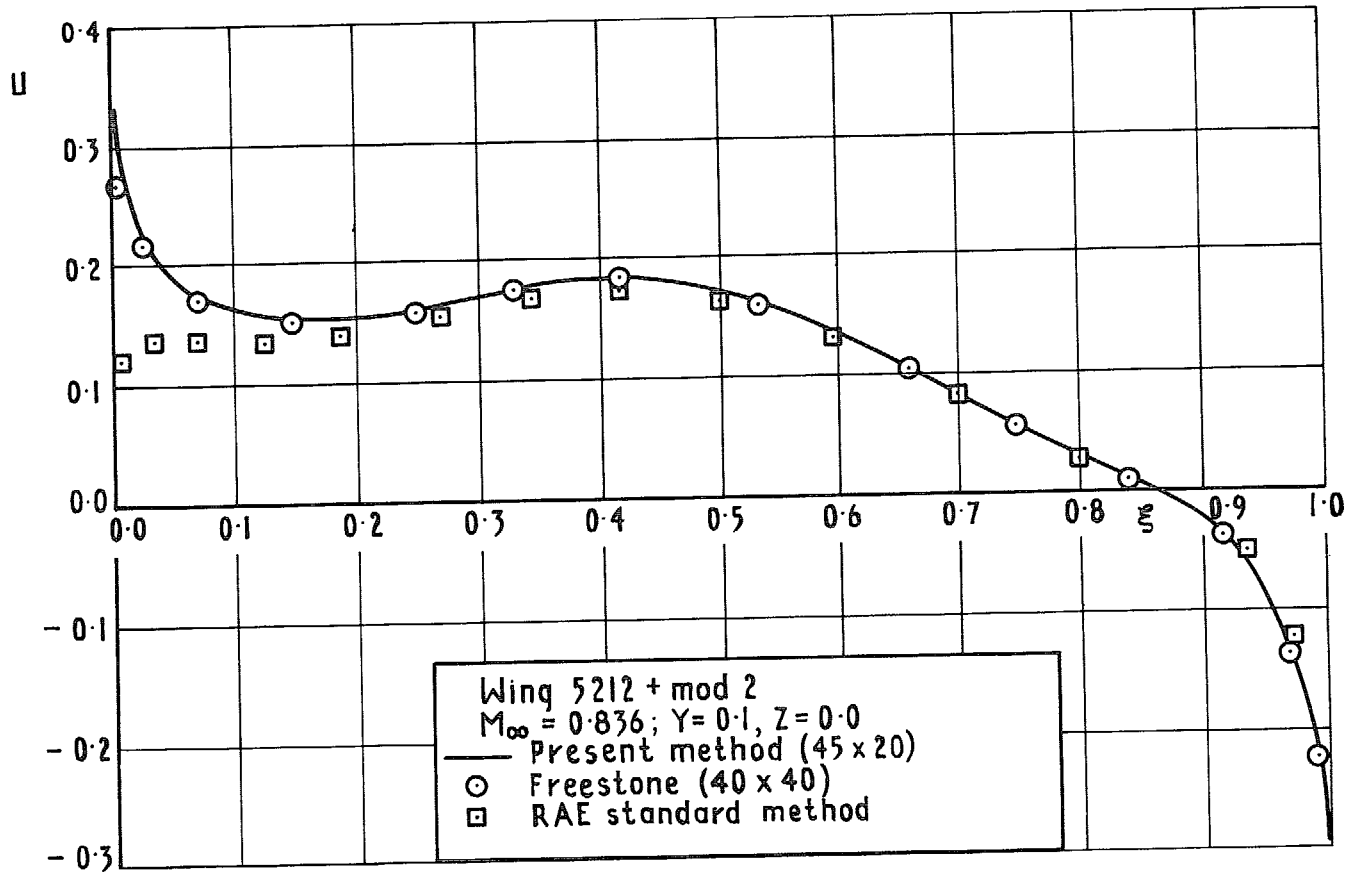

FIG. 14. Streamwise distribution of velocity on a wing with wing 'A' planform and R.A.E. (N.P.L.) 5212 section shape but modified in the root region: near root station.

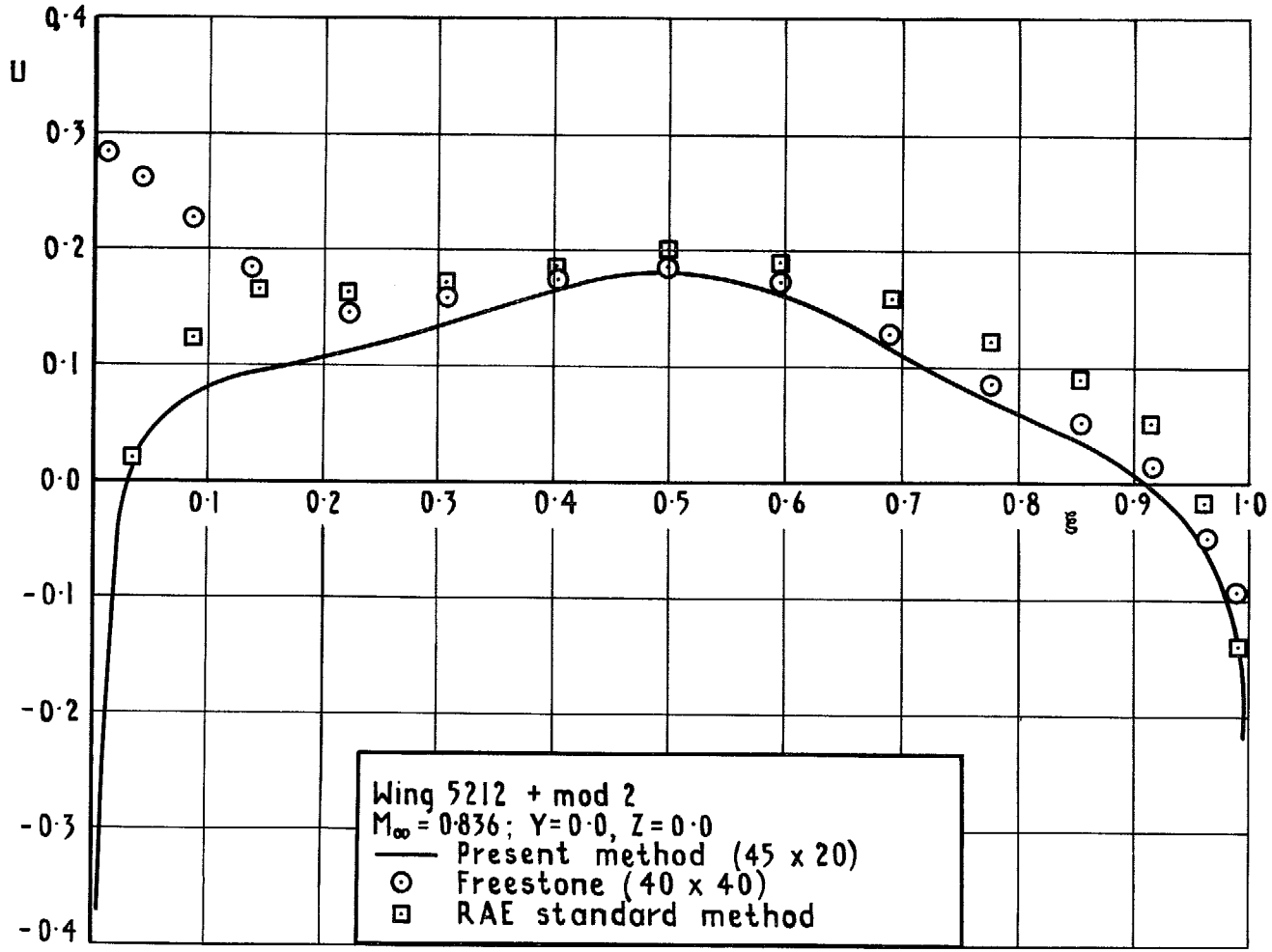

FIG. 15. Streamwise distribution of velocity on a wing with wing 'A' planform and R.A.E. (N.P.L.) 5212 section shape but modified in the root region: root station $Y = 0$.

Printed in England for Her Majesty's Stationery Office by J. W. Arrowsmith Ltd., Bristol BS3 2NT
Dd. 505374 K5 8/74

HER MAJESTY'S STATIONERY OFFICE

Government Bookshops

49 High Holborn, London WC1V 6HB
13a Castle Street, Edinburgh EH2 3AR
41 The Hayes, Cardiff CF1 1JW
Brazennose Street, Manchester M60 8AS
Southey House, Wine Street, Bristol BS1 2BQ
258 Broad Street, Birmingham B1 2HE
80 Chichester Street, Belfast BT1 4JY

Government publications are also available through booksellers

R. & M. No. 3751
ISBN 0 11 470844 4